

A Hybrid Transmitting and Reflecting Beyond Diagonal Reconfigurable Intelligent Surface with Independent Beam Control and Power Splitting

Zhaoyang Ming, *Student Member, IEEE*, Shanpu Shen, *Senior Member, IEEE*, Junhui Rao, *Member, IEEE*, Zan Li, *Student Member, IEEE*, Jichen Zhang, *Student Member, IEEE*, Chi Yuk Chiu, *Senior Member, IEEE*, and Ross Murch, *Fellow, IEEE*

Abstract—A hybrid transmitting and reflecting beyond diagonal reconfigurable intelligent surface (BD-RIS) design is proposed. Operating in the same aperture, frequency band and polarization, the proposed BD-RIS features independent beam steering control of its reflected and transmitted waves. In addition it provides a hybrid mode with both reflected and transmitted waves using tunable power splitting between beams. The BD-RIS comprises two phase reconfigurable antenna arrays interconnected by an array of tunable two-port power splitters. The two-port power splitter in each BD-RIS cell is built upon a varactor in parallel with a bias inductor to exert tunable impedance variations on transmission lines. Provided with variable reverse DC voltages, the two-port power splitter can control the power ratio of S_{11} over S_{21} from -20 dB to 20 dB, thus allowing tunable power splitting. Each antenna is 2-bit phase reconfigurable with 200 MHz bandwidth at 2.4 GHz so that each cell of BD-RIS can also achieve independent reflection and transmission phase control. To characterize and optimize the electromagnetic response of the proposed BD-RIS design, a Thévenin equivalent model and corresponding analytical method is provided. A BD-RIS with 4×4 cells was also prototyped and tested. Experiments show that in reflection and transmission mode, the fabricated BD-RIS can realize beam steering in reflection and transmission space, respectively. It is also verified that when operating in hybrid mode, the BD-RIS enables independent beam steering of the reflected and transmitted waves. This work helps fill the gap between realizing practical hardware design and establishing an accurate physical model for the hybrid transmitting and reflecting BD-RIS, enabling hybrid transmitting and reflecting BD-RIS assisted wireless communications.

Index Terms—BD-RIS, beam steering, reconfigurable intelligent surface (RIS), tunable power splitting, transmitting and reflecting beamforming.

I. INTRODUCTION

THE forthcoming sixth-generation (6G) mobile communication system is envisioned to provide extremely high data rates, high spectral- and energy-efficiency, extremely low

latency, and ubiquitous network coverage [1], [2]. Reconfigurable intelligent surfaces (RISs), are a promising technology for 6G, and have attracted significant attention. RISs consist of a large number of reconfigurable scattering elements and the electromagnetic response of each element can be smartly adjusted to manipulate the wireless environment [3]–[5].

On top of the conventional RISs, which are characterized by a diagonal scattering matrix, the novel concept of beyond diagonal RIS (BD-RIS) has been recently proposed [6], [7]. BD-RISs represent a family of RISs, where the adjacent elements can be interconnected through tunable impedance components, and can be characterized by a beyond diagonal scattering matrix, which provides more degrees-of-freedom to manipulate the wireless environment and thus brings an enhanced gain compared to conventional RISs [6]–[9].

One of the important BD-RIS modes is when it is configured to simultaneously transmit and reflect waves. When configured in this mode the BD-RIS is denoted here as a hybrid transmitting and reflecting BD-RIS and is also known in other literature as a simultaneously transmitting and reflecting RIS (STAR-RIS) [10] or intelligent omni-surface (IOS) [11]. Compared with conventional RISs which only support reflection from one side of the surface and provide half-space coverage only, the hybrid transmitting and reflecting BD-RIS supports simultaneous reflection and transmission from both sides of the surface and enables full-space coverage [6], [10]–[13]. The vast majority of the research performed on hybrid transmitting and reflecting BD-RIS has been devoted to system optimization [14], such as maximizing sum rate [8], [15], and enhancing spectral and energy efficiency [8], [16]. However, the limitation of these works [6], [8], [10]–[13], [15], [16] is that only numerical simulation is considered and there is no prototype design to experimentally verify the hybrid transmitting and reflecting BD-RIS.

Previously the implementation of bidirectional beam steering surfaces has been provided using metasurfaces [17]–[32], antennas [33]–[42], and frequency selective surfaces [43], [44]. To achieve independent transmitting and reflecting beam steering using a surface is however challenging. One approach has been to control the surface’s electromagnetic properties, including phases or amplitudes, by using different frequency bands for the transmitted and reflected waves [23]–[25], [39], [40], [44]. However, this approach is not suitable for wireless communication as spectrum efficiency is reduced due to the

This work was supported by Hong Kong Research Grants Council for the Area of Excellence Grant, AoE/E-601/22-R.

Zhaoyang Ming, Junhui Rao, Zan Li, Jichen Zhang and Chi Yuk Chiu are with the Department of Electronic and Computer Engineering, University of Hong Kong Science and Technology, Hong Kong. (e-mail: zming@connect.ust.hk, jr000a@connect.ust.hk).

Shanpu Shen is with the Department of Electrical Engineering and Electronics, University of Liverpool, Liverpool, U.K. (e-mail: Shanpu.Shen@liverpool.ac.uk).

R. Murch is with the Department of Electronic and Computer Engineering and Institute for Advanced Study (IAS) at the Hong Kong University of Science and Technology, Hong Kong. (e-mail: eermurch@ust.hk).

need for two frequency bands. An alternative approach to achieve independent beam control is to utilize polarization multiplexing to respectively control the transmitting and reflecting beams at two orthogonal polarizations [18], [26]–[29], [41], [42]. However this is not conducive for extensions to dual-polarization designs and has the issue of polarization conversion [32], [34]–[36]. In addition to frequency and polarization multiplexing, exploiting spatial multiplexing such as different propagation directions [29]–[31], can be used to respectively control the reflected and transmitted beams. However, using spatial multiplexing comes at the cost of structural symmetry. That is when excited by incident waves with the same electromagnetic properties from opposing directions, the designed surface may not maintain the same functionality or operate normally as it does when approached from the original direction. More importantly, many of the abovementioned designs [21], [23]–[29], [31], [32], [39]–[42], have their corresponding functions and properties entirely fixed once fabricated, and cannot be changed or reconfigured, greatly limiting their application in real-time wireless communication systems which require adaptation.

In addition to the aforementioned limitations of frequency, polarization, spatial multiplexing, and reconfigurability, there is also the issue that independent and flexible mode switching between reflection, transmission, and hybrid modes has not been fully implemented. Although some designs have allowed for dynamic switching between reflection and transmission modes [17], [19], [22], [35], [38] and achieved bidirectional functionality by using aperture multiplexing techniques [19], [22], [35], the issue is that a single unit cannot directly realize mode switching and arbitrary power splitting. Therefore, it remains a challenge to design hybrid transmitting and reflecting BD-RIS to implement independent beam control and mode switching with arbitrary power splitting between beams.

To overcome the aforementioned challenges, in this work we propose a highly reconfigurable hybrid transmitting and reflecting BD-RIS with independent beam control and power splitting with mode switching in the same frequency band, polarization, and aperture with a symmetric structure. An overview of the proposed BD-RIS with 4×4 cells is shown in Fig. 1, where two 4×4 phase reconfigurable antenna arrays are interconnected via 16 tunable two-port power splitters. The phase states of all antennas and the operation mode of the power splitters are controlled by field-programmable gate arrays (FPGAs) and a DC power supply, respectively. By setting the operation mode of the power splitters and configuring all the antennas with the desired phases, we can realize dynamic mode switching with independent beam steering of the reflected and transmitted beams. This work fills the gap between realizing practical hardware design and establishing an accurate physical model for the hybrid transmitting and reflecting BD-RIS, helping enable hybrid transmitting and reflecting BD-RIS assisted wireless communications. The contributions of this work are summarized as follows.

1) *Hardware Design Requirements*: We propose and justify the hardware design requirements for each BD-RIS cell. Our proposed requirement is that each cell should achieve at least eight reconfigurable states, including two states for reflection

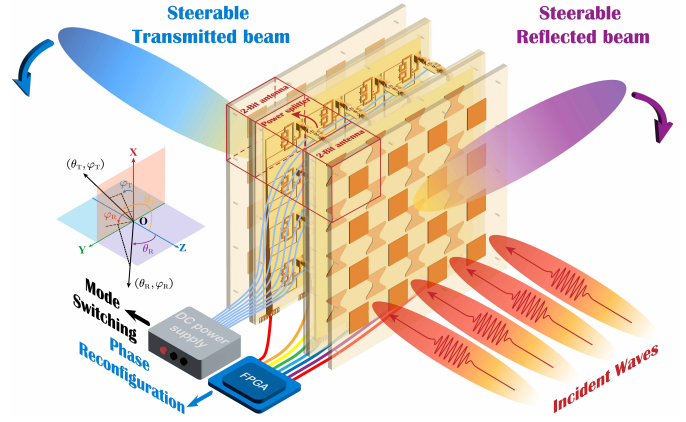


Fig. 1. Illustration of the proposed hybrid transmitting and reflecting BD-RIS with 4×4 cells. In this example waves incident from the right hand side can be all reflected, all transmitted or simultaneously transmitted and reflected in a hybrid mode.

mode, two for transmission mode and at least four states for hybrid mode to enable independent beam control and mode switching.

2) *Hardware Design Methodology and Architecture*: Based on the proposed design requirements, we propose a multiple-module-integrated architecture for BD-RIS. This architecture is formed by interconnecting two 2-bit phase reconfigurable antennas with a tunable two-port power splitter, thus leading to a symmetrical structure and maintaining the same polarization for all reflected and transmitted waves.

3) *Physical Model, Analytical Method, and Optimization*: We establish the corresponding Thévenin equivalent model for the proposed architecture and derive an analytical method to efficiently calculate the reflected and transmitted waves of the proposed BD-RIS under plane wave excitation. The genetic algorithm (GA) is used to produce beamforming designs.

4) *Prototype and Experimental Verification*: We fabricate a hybrid transmitting and reflecting BD-RIS prototype with 4×4 cells and build up a testbed to measure the reflected and transmitted scattered patterns to verify its multifunctionalities.

This paper is organized as follows. Section II introduces the model for the hybrid transmitting and reflecting BD-RIS as proposed for wireless communications. Section III elaborates the design specification and the cell design methodology. Section IV illustrates the design and implementation of multiple modules used in each cell of BD-RIS, including a two-port power splitter and a 2-bit phase reconfigurable antenna. Section V builds up the physical model and describes the analytical and beamforming optimization methods for the proposed BD-RIS. Section VI provides experimental verification using a prototype of the proposed BD-RIS with 4×4 cells, and discussions. Finally, Section VII concludes this work.

II. BD-RIS BACKGROUND

We consider a hybrid transmitting and reflecting BD-RIS which consists of M cells as shown in Fig. 2. The m th cell, for $m \in \mathcal{M} = \{1, \dots, M\}$, is constructed by antenna m

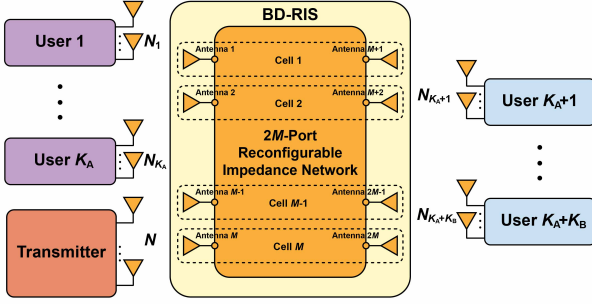


Fig. 2. System diagram of an M -cell BD-RIS-aided communication system.

and antenna $m + M$ connected to a two-port reconfigurable network, whose scattering matrix is denoted as

$$\mathbf{S}_m = \begin{bmatrix} \phi_{r,m} & \phi_{t,m} \\ \phi_{t,m} & \phi_{r,m+M} \end{bmatrix}, \quad (1)$$

where the subscript r refers to the reflection scattering parameter and the subscript t refers to the transmission scattering parameter between the m and $m + M$ ports (and also by symmetry the $m + M$ and m ports). When the two-port reconfigurable network is lossless, $\phi_{r,m}$ and $\phi_{t,m}$ should satisfy

$$|\phi_{r,m}|^2 + |\phi_{t,m}|^2 = 1, \forall m \in \mathcal{M}, \quad (2)$$

and this arises from energy conservation for reflection and transmission.

The entire M -cell hybrid transmitting and reflecting BD-RIS contains $2M$ antennas and a $2M$ -port reconfigurable network. Using the notation in (1), the scattering matrix $\Phi \in \mathbb{C}^{2M \times 2M}$ of the entire $2M$ -port reconfigurable network can be written as,

$$[\Phi]_{i,j} = \begin{cases} \phi_{r,i} & , \text{for } i = j, \\ \phi_{t,i} & , \text{for } j - i = M, \\ \phi_{t,j} & , \text{for } i - j = M, \\ 0 & , \text{otherwise.} \end{cases} \quad (3)$$

This scattering matrix has both diagonal and off-diagonal elements, and that is why it is referred to as a BD-RIS [6]. Using (3) the complete channel model for the hybrid transmitting and reflecting BD-RIS system can also be developed as described in [6].

In the hybrid transmitting and reflecting BD-RIS, each antenna has a uni-directional radiation pattern and the two antennas in each cell are back to back, so that each antenna covers a half space (which we refer to as a sector in the remainder of the paper) as shown in Fig. 3. We denote the two sectors as, sector A, and it contains antennas 1 to M and sector B which contains antennas $M + 1$ to $2M$. We assume that the transmitter and K_A users, indexed by $\mathcal{K}_r = \{1, \dots, K_A\}$, $0 < K_A < K$, are located in sector A (and therefore where the BD-RIS reflected waves are present), and the remaining $K_B = K - K_A$ users, indexed by $\mathcal{K}_t = \{K_A + 1, \dots, K\}$, are located in sector B (and where the BD-RIS transmitted waves are present). Since our proposed BD-RIS structure is completely symmetric, the reverse configuration (transmitter

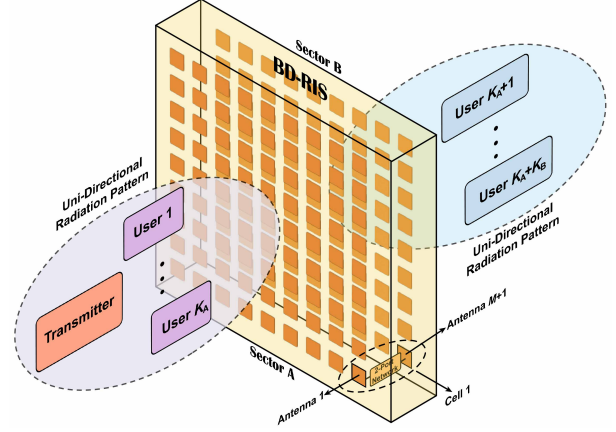


Fig. 3. An M -cell BD-RIS with $2M$ back to back uni-directional antennas partitioning the whole space into reflection (sector A) and transmission (sector B) half spaces.

in sector B) is also automatically satisfied and therefore we do not consider the return loss $\phi_{r,i}$ for $i > M$ further.

Based on the relation (2), we can adjust the phase $\theta_{r,m} = \arg(\phi_{r,m})$ and $\theta_{t,m} = \arg(\phi_{t,m})$, $\forall m \in \mathcal{M}$ to control the beams for reflection and transmission, respectively. On the other hand, we can adjust the magnitude $|\phi_{r,m}|$ and $|\phi_{t,m}|$, $\forall m \in \mathcal{M}$ to control the power allocation for reflection and transmission under the constraint (2).

III. BD-RIS CELL DESIGN METHODOLOGY

In this section, we propose and specify the hardware design requirements for each cell of the hybrid transmitting and reflecting BD-RIS and propose a multiple-module-integrated architecture based on scattering matrix analysis.

A. Design Specification

To obtain the optimal performance, an ideal hybrid transmitting and reflecting BD-RIS should be able to continuously adjust the phase and magnitude of $\phi_{r,m}$ and $\phi_{t,m}$, $\forall m \in \mathcal{M}$. This is very challenging in practice and as a compromise we discretize the magnitude and phase of $\phi_{r,m}$ and $\phi_{t,m}$ and use RF switches to implement the hybrid transmitting and reflecting BD-RIS. Furthermore, to reduce circuit complexity and insertion loss resulting from RF switches in practice, we also restrict the configurations to the following three modes:

1) *Reflection Mode*: Each cell purely reflects an incident electromagnetic wave with at least 1-bit phase reconfigurability, i.e. $|\phi_{r,m}| \approx 1$, $|\phi_{t,m}| \approx 0$, $\theta_{r,m} \in \{0, \pi\}$, $\forall m \in \mathcal{M}$.

2) *Transmission Mode*: Each cell purely transmits an incident electromagnetic wave with at least 1-bit phase reconfigurability, i.e. $|\phi_{r,m}| \approx 0$, $|\phi_{t,m}| \approx 1$, $\theta_{t,m} \in \{0, \pi\}$, $\forall m \in \mathcal{M}$.

3) *Hybrid Mode*: Each cell can both reflect and transmit an incident electromagnetic wave with equal power. Therefore, half of the incident electromagnetic wave is reflected and the other half is transmitted both with at least 1-bit independent phase reconfigurability, i.e. $|\phi_{r,m}| \approx \frac{1}{\sqrt{2}}$, $|\phi_{t,m}| \approx \frac{1}{\sqrt{2}}$, $\theta_{r,m} \in \{0, \pi\}$, $\theta_{t,m} \in \{0, \pi\}$, $\forall m \in \mathcal{M}$.

To achieve these three modes and enable independent beam control, each cell should achieve at least eight reconfigurable

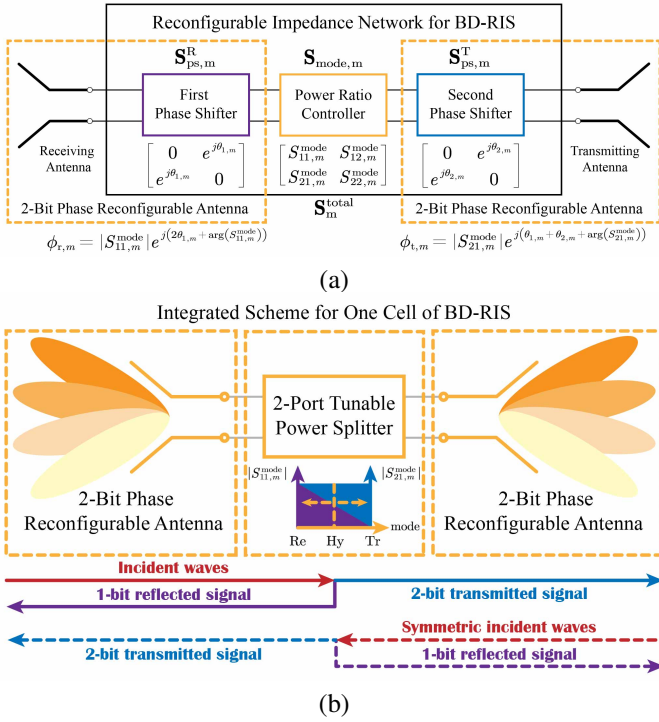


Fig. 4. The proposed architecture for a single cell of the hybrid transmitting and reflecting BD-RIS. (a) A single cell of BD-RIS containing reconfigurable impedance network. (b) Integrated scheme for a single cell of BD-RIS. Re: Reflection, Hy: Hybrid, Tr: Transmission.

states. This includes two states for the reflection mode, two for the transmission mode and at least four states for the hybrid mode.

B. Cell Design

To realize the design specification, we propose a two-port reconfigurable impedance network for each cell of the hybrid transmitting and reflecting BD-RIS as shown in Fig. 4(a). Each two-port reconfigurable impedance network consists of three cascaded modules, including two phase shifters responsible for phase reconfigurability of the reflected and transmitted waves, and one power splitter responsible for dynamic mode switching. For the m th cell, each of these modules is equivalent to a two-port network and the scattering matrices for the first and second phase shifter and the power splitter can be expressed respectively as

$$\mathbf{S}_{ps,m}^R = \begin{bmatrix} 0 & e^{j\theta_{1,m}} \\ e^{j\theta_{1,m}} & 0 \end{bmatrix}, \quad (4)$$

$$\mathbf{S}_{ps,m}^T = \begin{bmatrix} 0 & e^{j\theta_{2,m}} \\ e^{j\theta_{2,m}} & 0 \end{bmatrix}, \quad (5)$$

$$\mathbf{S}_{mode,m} = \begin{bmatrix} S_{11,m}^{mode} & S_{12,m}^{mode} \\ S_{21,m}^{mode} & S_{22,m}^{mode} \end{bmatrix}, \quad (6)$$

where $\theta_{1,m}$ and $\theta_{2,m}$ are the phase shifts introduced by the two phase shifters and $S_{ij,m}^{mode}$, $\forall i, j \in \{1, 2\}$ are the S-parameters of the power splitter in the m th cell, $\forall m \in \mathcal{M}$. The total

scattering matrix $\mathbf{S}_m^{\text{total}}$ of the m th reconfigurable impedance network can be found as

$$\mathbf{S}_m^{\text{total}} = \begin{bmatrix} S_{11,m}^{mode} e^{j2\theta_{1,m}} & S_{12,m}^{mode} e^{j(\theta_{1,m} + \theta_{2,m})} \\ S_{21,m}^{mode} e^{j(\theta_{1,m} + \theta_{2,m})} & S_{22,m}^{mode} e^{j2\theta_{2,m}} \end{bmatrix}. \quad (7)$$

Denoting $S_{11,m}^{mode} = |S_{11,m}^{mode}| e^{jc_{1,m}}$ and $S_{21,m}^{mode} = |S_{21,m}^{mode}| e^{jc_{2,m}}$, where $c_{1,m} = \arg(S_{11,m}^{mode})$ and $c_{2,m} = \arg(S_{21,m}^{mode})$, and comparing (7) with (1), we have that

$$\phi_{r,m} = S_{11,m}^{\text{total}} = |S_{11,m}^{mode}| e^{j(2\theta_{1,m} + c_{1,m})}, \quad (8)$$

$$\phi_{t,m} = S_{21,m}^{\text{total}} = |S_{21,m}^{mode}| e^{j(\theta_{1,m} + \theta_{2,m} + c_{2,m})}. \quad (9)$$

Therefore, for the m th cell of the hybrid transmitting and reflecting BD-RIS, the phase shifts of the reflected and transmitted signals, and the power ratio of reflected signals over the transmitted waves can be expressed respectively as

$$\theta_{r,m} = 2\theta_{1,m} + c_{1,m}, \quad (10)$$

$$\theta_{t,m} = \theta_{1,m} + \theta_{2,m} + c_{2,m}, \quad (11)$$

$$\left| \frac{\phi_{r,m}}{\phi_{t,m}} \right|^2 = \left| \frac{S_{11,m}^{mode}}{S_{21,m}^{mode}} \right|^2. \quad (12)$$

As specified in Section III.A and based on the reflection and transmission phase relationship (10) and (11), to realize at least 1-bit independent phase reconfigurability between $\theta_{r,m}$ and $\theta_{t,m}$, and for structural symmetry consideration, the phase tunability of these two phase shifters should be at least 2-bit, that is, $\theta_{1,m}, \theta_{2,m} \in \{0, \frac{\pi}{2}, \pi, \frac{3\pi}{2}\}$. In this case, the hybrid transmitting and reflecting BD-RIS can always achieve 1-bit independent control for the reflected waves and 2-bit independent control for the transmitted waves, regardless of the direction from which the incident wave arrives. Moreover, to realize dynamic mode switching, we need to reconfigure the two-port power splitter so that the power ratio given by (12) can be tuned to 0, 1, and to $\gg 1$, which corresponds to the three modes specified in Section III.A.

In this way, $\mathbf{S}_{mode,m}$ is fixed for a specific mode accordingly, and as expressed from (10) to (12), the phase reconfigurability of $\theta_{r,m}$ and $\theta_{t,m}$ is only related to those two phase shifters via $\theta_{1,m}$ and $\theta_{2,m}$. Furthermore, the phase reconfiguration will not affect the power ratio. It should also be noted that by cascading this two-port network with the same polarization port of the reflecting and transmitting antenna, our design also avoids introducing polarization conversion.

Also note that implementing two extra phase shifters with 2-bit phase reconfigurability will make the reconfigurable impedance network too bulky to be integrated with two antennas, and cause extra amplitude variation for different phase states, thereby affecting the power ratio controlling. Therefore, for the consideration of reducing energy loss and making the design compact, we incorporate those 2-bit phase shifters into the antennas. Namely to design two 2-bit phase reconfigurable antennas for each cell. Our proposed scheme for one cell of the hybrid transmitting and reflecting BD-RIS can then be depicted by Fig. 4(b), which is a symmetrical and integrated scheme involving no polarization conversion.

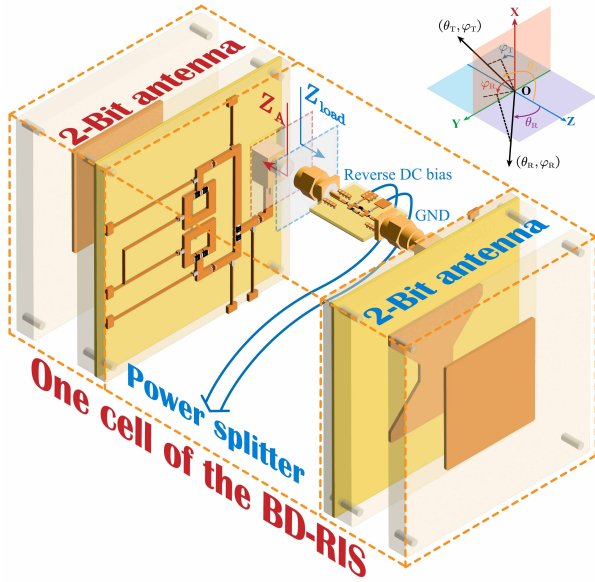


Fig. 5. One cell of the hybrid transmitting and reflecting BD-RIS including two 2-bit phase reconfigurable antennas and a two-port tunable power splitter.

IV. BD-RIS CELL IMPLEMENTATION

In this section, we provide details of the BD-RIS cell implementation that meets the design criteria developed in Section III. Prototypes and measurements are also provided.

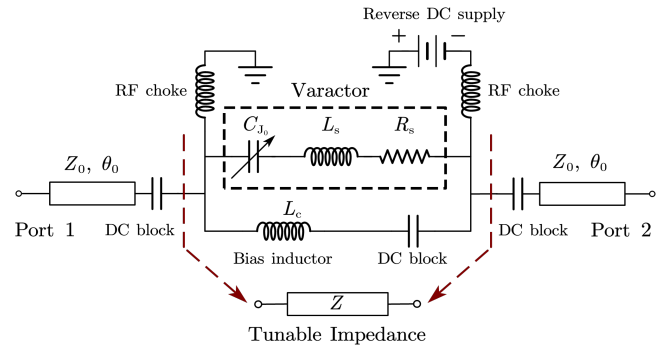
A. Overall Cell Architecture

The specific structure based on the proposed scheme in Fig. 4(b) is shown in Fig. 5 for one cell of the hybrid transmitting and reflecting BD-RIS. As illustrated, each cell is composed of three cascaded modules, including one 2-bit phase reconfigurable antenna serving as the reflecting antenna, a tunable two-port power splitter and another 2-bit phase reconfigurable antenna serving as the transmitting antenna. As mentioned, implementing the same 2-bit antennas on both sides makes the architecture symmetrical. In addition, two SMA connectors with 90° right-angle bends are used to achieve the vertical transitions from the microstrip line circuit of the antenna to that of the power splitter at two sides. Details of how we design these modules are elaborated in the following subsections.

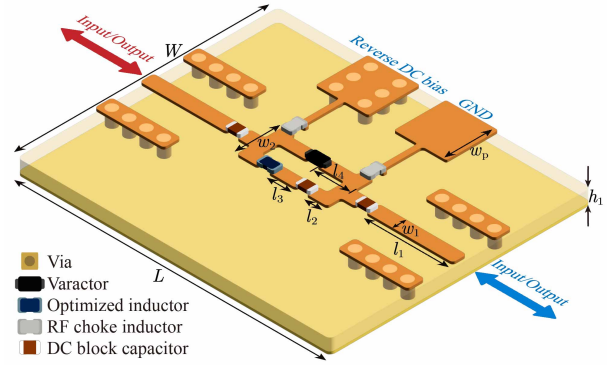
B. Tunable Two-port Power Splitter

As shown in Fig. 4(b), our objective is to design a tunable two-port power splitter to realize mode switching. Based on the idea of utilizing reconfigurable components to exert impedance variations on the transmission lines, we propose a straightforward two-port network as shown in Fig. 6(a), where a tunable component of impedance Z is embedded in series with two transmission lines with characteristic impedance Z_0 . The corresponding scattering matrix \mathbf{S}_{mode} of this two-port network is given by

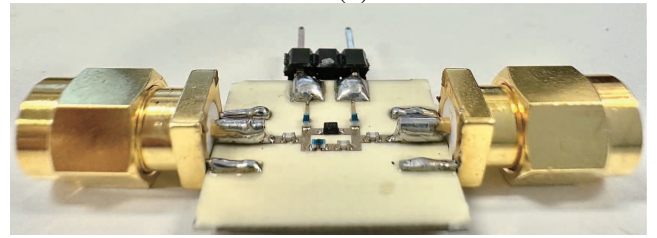
$$\mathbf{S}_{\text{mode}} = \frac{1}{Z + 2Z_0} \begin{bmatrix} Z & 2Z_0 \\ 2Z_0 & Z \end{bmatrix}. \quad (13)$$



(a)



(b)



(c)

Fig. 6. Tunable two-port power splitter design for a BD-RIS cell. (a) Schematic of the two-port tunable power splitter. (b) Overall structure. The dimensions are $W = 13.5$, $L = 18$, $h_1 = 0.813$, $l_1 = 5$, $l_2 = 1.2$, $l_3 = 1.6$, $l_4 = 2.3$, $w_1 = 0.7$, $w_2 = 2.4$, $w_p = 3$ (unit: mm). Light yellow color: dielectric layer. Dark orange color: copper. Yellow color: ground. (c) Photograph of the fabricated two-port power splitter.

Given Z_0 as 50Ω , we can simplify the power ratio of the reflected signal over the transmitted signal as

$$P = 20 \log \left| \frac{S_{11}^{\text{mode}}}{S_{21}^{\text{mode}}} \right| = 20 \log \left| \frac{Z}{100} \right| \text{ dB}. \quad (14)$$

To achieve switching between transmission, hybrid, and reflection modes, as proposed in Section III.A, we can set the tuning range for the power ratio P , to -20 dB, 0 dB, and to 20 dB. Correspondingly, the tunable range of Z should at least satisfy $|Z| \in [10, 10^3]$. Setting the center frequency as 2.4 GHz, and considering that the adjustable capacitance range of commonly used commercial varactors is from a few tenths of a picofarad (pF) to tens of pF, we propose the circuit structure shown in Fig. 6(a) to achieve the required equivalent impedance tuning capability for dynamic mode switching. Specifically, a commercial varactor SMV2020-079LF from

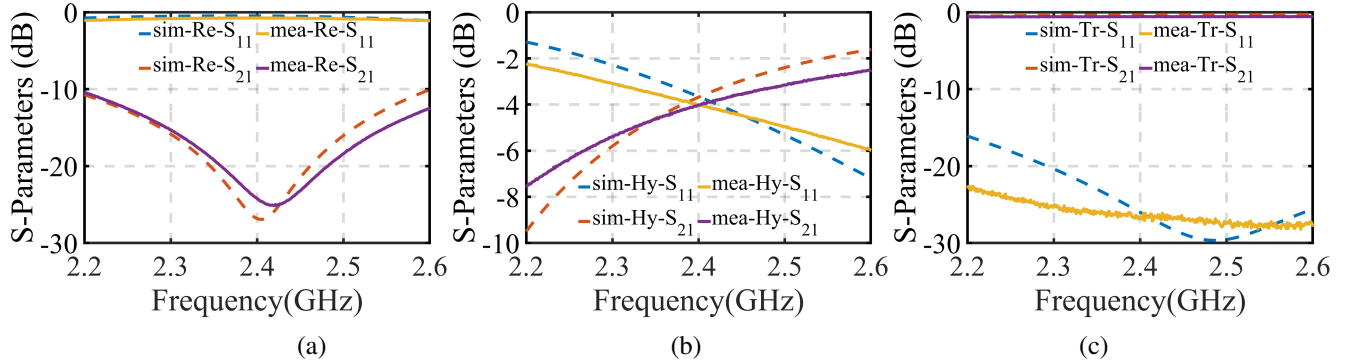


Fig. 7. Performance of the fabricated two-port power splitter when the reverse DC voltage is set as -10.8 V, -7.4 V, and 0 V, which respectively corresponds to: (a) Reflection mode; (b) Hybrid mode; (c) Transmission mode.

Skyworks is connected in parallel with a carefully chosen bias inductor 0402DC-3N9XJRW from Coilcraft to form the core part of the two-port power splitter. The tunable impedance Z can then be given by

$$Z = \frac{\left(\frac{1}{j\omega C_{J_0}} + j\omega L_s + R_s \right) j\omega L_c}{\frac{1}{j\omega C_{J_0}} + j\omega L_s + R_s + j\omega L_c}, \quad (15)$$

where $0.35 \text{ pF} \leq C_{J_0} \leq 3.2 \text{ pF}$ is the tunable capacitance of varactor SMV2020-079LF when provided with reverse voltage from -20 V to 0 V. The series parasitic inductance L_s and resistance R_s introduced by the package and transistor is 0.7 nH and 2.5Ω , respectively. The inductance of the parallel inductor L_c is optimized as 3.9 nH. This provides crucial admittance bias for the tunable admittance range of the varactor so that the corresponding $|Z|$ can fulfill the requirements for dynamic mode switching. Specifically, the designed tunable two-port power splitter is implemented on a Rogers 4003C substrate ($\epsilon_r = 3.55$ and $\tan \delta = 0.0027$) with a thickness of 0.813 mm as shown in Fig. 6(b). Except for the above mentioned essential components, other components include two inductors 0402DC-R10XGRW from Coilcraft serving as the RF chokes and three capacitors GJM1555C1H130GB01D from Murata serving as the DC chokes.

The fabricated circuit is shown in Fig. 6(c), and it was measured by a calibrated Rohde & Schwarz ZVA40 4-Port vector network analyzer. As demonstrated in Fig. 7(a)-(c), by setting reverse DC voltage V_p as -10.8 V, -7.4 V, and 0 V, using a 50-watt E3620A dual-output power supply, we can realize mode switching between reflection, hybrid and transmission modes, respectively. The measured insertion loss for the reflection and transmission modes at 2.4 GHz is less than 0.8 dB, which is around 0.3 dB larger than simulated results due to extra loss introduced by SMA connectors and cables. The simulated S_{11} and S_{21} for the hybrid mode at 2.4 GHz are -3.68 dB and -3.66 dB, while the measured S_{11} and S_{21} are -4.01 dB and -4.02 dB, which shows that equal power splitting can be approximately obtained. Besides, it can be seen from Fig. 7(b) that the 1-dB variation bandwidth for hybrid mode is from 2.35 GHz to 2.45 GHz.

C. 2-Bit Phase Reconfigurable Antenna

It is useful here, and also later in the experimental section, to define the structural and antenna scattering of antennas. When electromagnetic waves impinge on the surface of an antenna, the scattered pattern can be decomposed into structural and antenna scattering parts. The structural scattering part is defined here as the scattered pattern when the antenna is perfectly conjugate matched. The antenna scattering counterpart is then defined as that part of the radiation pattern that arises when the load deviates from the conjugate match. As illustrated in [45], [46], the scattered pattern $E^s(Z_{\text{load}})$ when the antenna is terminated with a load Z_{load} can be expressed as

$$E^s(Z_{\text{load}}) = E^s(Z_A^*) - \frac{\Gamma^* Z_A I_s E^{\text{unit}}}{2R_A}, \quad (16)$$

where Z_A^* is the perfect conjugate match of the antenna input impedance Z_A , R_A is the real part of Z_A , and I_s is the current induced by the incident wave at the antenna's port when the port is shorted. E^{unit} is the radiation pattern when the antenna is excited by a unit current at the input port. Γ^* is related to Z_{load} by

$$\Gamma^* = \frac{Z_{\text{load}} - Z_A^*}{Z_{\text{load}} + Z_A^*}, \quad (17)$$

This leads to the typical approach to achieve reconfiguration in which changing the load of the antenna will alter the antenna scattering.

The novelty in our design is that we alter the antenna scattering part by changing the current I_s and E^{unit} . This is performed by integrating a 2-bit phase shifter into the antenna structure. The advantage of this approach is that there is less loss, because there is no need for a load and its transmission line. In addition it enables a much more compact design.

Based on the above observations, the overall geometry of the proposed 2-bit phase reconfigurable antenna is shown in Fig. 8(a), which consists of three dielectric layers and four metallic layers. The bottom metallic layer is the microstrip feeding network integrated with three pairs of switches to realize 2-bit phase reconfigurability. The specific circuit topology is shown in Fig. 8(b). By selecting one of the first pair of switches, S1 and S2, that are embedded on two transmission line paths with a quarter-wavelength electrical length difference, a 90°

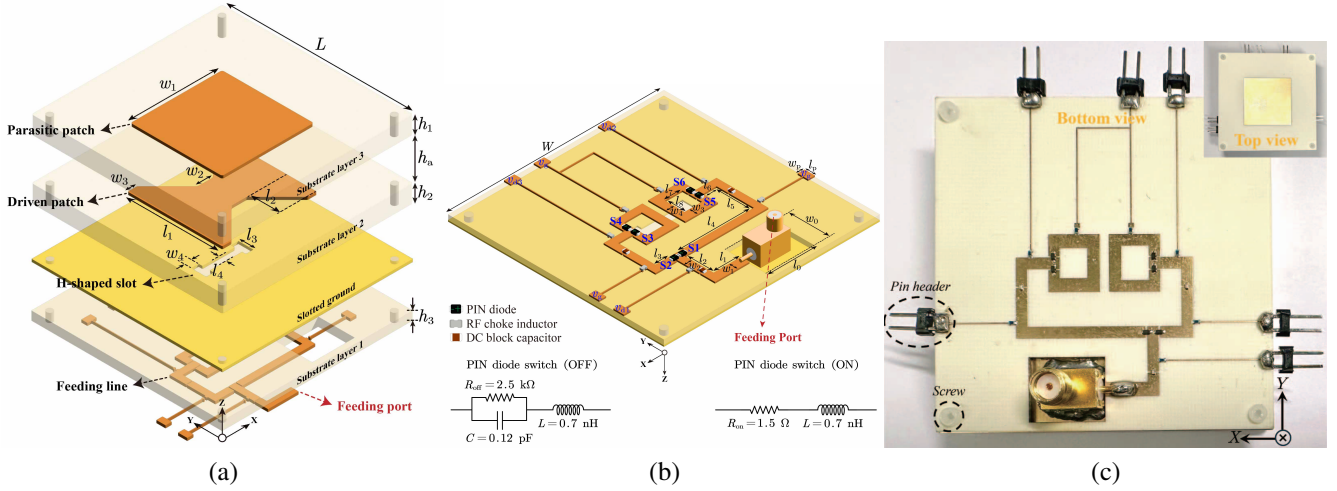


Fig. 8. 2-Bit phase reconfigurable antenna design for the proposed BD-RIS. (a) Overall structure of the designed aperture coupled phase reconfigurable antenna. The dimensions are $L = 62.5$, $h_1 = 3.048$, $h_2 = 3.048$, $h_3 = 1.524$, $h_a = 8$, $w_1 = 30$, $w_2 = 5$, $w_3 = 3$, $w_4 = 2.5$, $l_1 = 31$, $l_2 = 10$, $l_3 = 5$, $l_4 = 2.5$ (unit: mm). (b) Schematic of the integrated 2-bit phase shifter design and equivalent circuit models for the on and off states of diode SMP1345-079LF. The dimensions are $W = 62.5$, $w_0 = 12$, $w_1 = 2.5$, $w_2 = 2.1$, $w_3 = 2.5$, $w_4 = 2.3$, $w_p = 2$, $l_0 = 14$, $l_1 = 7.9$, $l_2 = 8.3$, $l_3 = 4$, $l_4 = 7.9$, $l_5 = 8.3$, $l_6 = 4$, $l_7 = 5.1$, $l_8 = 5.7$, $l_p = 3$ (unit: mm). Light yellow color: dielectric layer. Dark orange color: copper. Yellow color: ground. (c) Photograph of the fabricated 2-bit antenna.

phase difference can then be achieved. Furthermore, at the end of each path, there is a split ring mounted with another pair of switches, S3 and S4 or S5 and S6. Similarly, by selecting one of the pair of switches, the current flowing through the split ring will be reversed, thus generating a 180° phase difference. By properly controlling three pairs of switches as shown in Table I, we can realize 2-bit phase reconfigurability by controlling I_s and E^{unit} in (16).

The RF switch we use is the diode SMP1345-079LF from Skyworks and its equivalent circuit models for the on and off states are shown in Fig. 8(b). Each pair of switches are mounted in series on three branches of transmission lines and the left and right branches are always connected to the reference ground plane whose voltage V_g is kept as 0 V. The DC bias voltage V_{di} , for $i = 1, 2, 3$, is then added on the center branch and when $V_{di} = 1.6$ V, the corresponding diode S1 or S3 or S5 will be turned on, and the counterpart S2 or S4 or S6 will be turned off. When $V_{di} = -1.6$ V, the situation is the opposite. When $V_{di} = 0$ V, then no diode will be turned on. By properly controlling three pairs of switches as shown in Table I, we can then realize 2-bit phase reconfigurability. It should be noted that, V_{d1} can be provided by a single I/O pin (3.3-/0-V output) of a commercial FPGA whose GND is biased to be -1.6 V. While to provide three states of bias voltages for V_{d2} or V_{d3} , we connect two I/O pins in parallel, so that by assigning one of the output as 1.6 V, another one as -1.6 V, or both of the two outputs as 1.6 V, or -1.6 V, we can control the parallel output as 0 V, 1.6 V, and -1.6 V, respectively. Hence, for a single 2-bit antenna, it should be controlled by 5 I/O pins.

To improve the bandwidth of the patch antenna, we implement the aperture coupled technique, reshape the slot coupled square patch into a bowtie-like and introduce another layer of parasitic patch separated by an air gap of height h_a . All three dielectric layers are Rogers 4003C ($\epsilon_r = 3.55$,

TABLE I
STATES OF THE 2-BIT PHASE RECONFIGURABLE ANTENNA

States	S1	S2	S3	S4	S5	S6	Phase
00	ON	OFF	ON	OFF	OFF	OFF	0°
01	OFF	ON	OFF	OFF	OFF	ON	90°
10	ON	OFF	OFF	ON	OFF	OFF	180°
11	OFF	ON	OFF	OFF	ON	OFF	270°

$\tan \delta = 0.0027$), where the upper two layers are of a thickness of 3.048 mm and the bottom layer is 1.524 mm. The upper two metallic layers are the parasitic patch and bowtie-like patch radiators. The third metallic layer is the slotted ground plane, which couples energy from the lower microstrip feeding network to the upper patch radiators.

The simulated and measured S_{11} parameters of the fabricated 2-bit antenna is shown in Fig. 9(a) and (b), respectively. Despite a slight frequency shift for state 01 and state 11 due to fabrication error, the measured S-parameters of the four states are generally in good agreement with the simulated results and the bandwidth around 2.4 GHz is over 200 MHz (2.3-2.5 GHz). Fig. 9(c)-(f) demonstrate the simulated and measured E-plane (XOZ plane) and H-plane (YOZ plane) radiation patterns of the four states at 2.4 GHz, respectively. The radiation patterns and broadside co-polarization gains among the four states are very similar and stable. Fig. 9(g) and (h) depicts the simulated and measured E-field phase responses of four states at 2.4 GHz, where the four phases are evenly distributed over 360° with a 90° phase difference between adjacent states. Therefore, a 2-bit phase reconfigurable antenna design showing favorable performance for the proposed BD-RIS architecture is achieved.

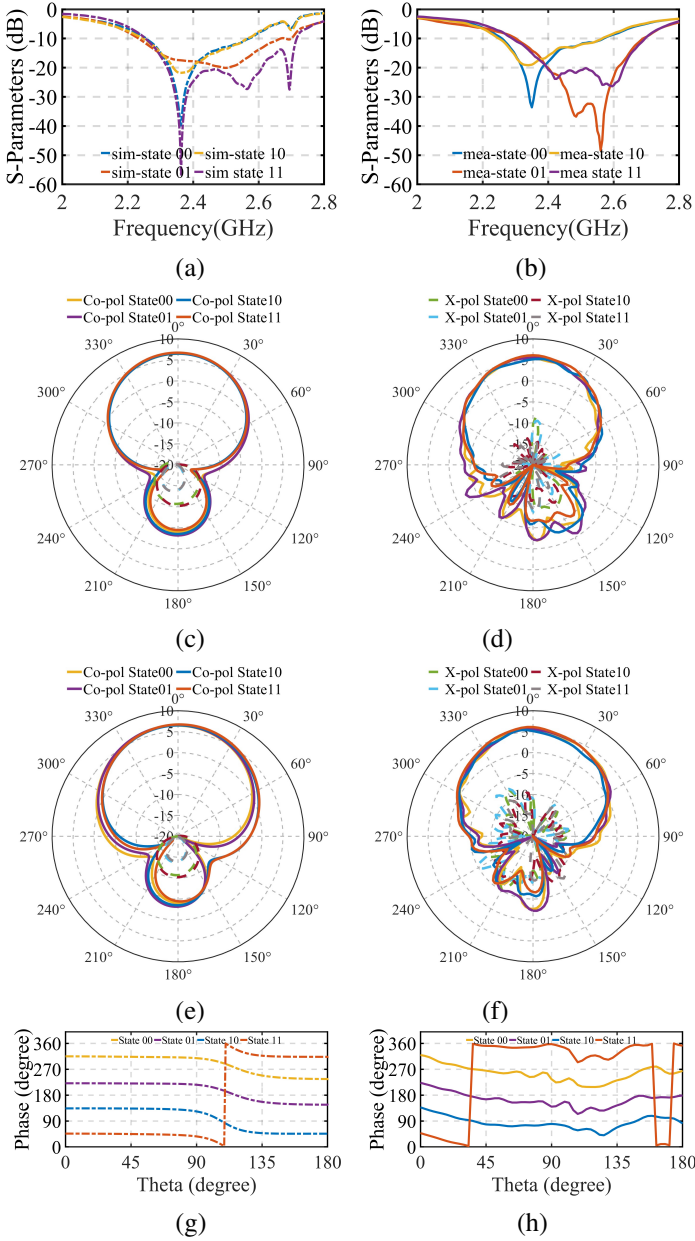


Fig. 9. Performance of the fabricated 2-bit phase reconfigurable antenna. (a) Simulated input return loss. (b) Measured input return loss. (c) Simulated radiation pattern in the E plane (unit: dBi). (d) Measured radiation pattern in the E plane (unit: dBi). (e) Simulated radiation pattern in the H plane (unit: dBi). (f) Measured radiation pattern in the H plane (unit: dBi). (g) Simulated E-field phase responses. (h) Measured E-field phase responses.

V. MULTIPLE CELLS PERFORMANCE ANALYSIS

In this section we establish models and perform analysis to characterize the performance of the reflection and transmission electromagnetic responses of our BD-RIS with multiple cells. Subsequently, we employ the genetic algorithm (GA) to conduct beamforming optimization for our proposed BD-RIS under different operation modes.

A. Physical Model and Analytical Method

Physical models have been proposed to model the electromagnetic responses of a hybrid transmitting and reflecting

BD-RIS, such as the phase shift model, the load impedance model and the generalized sheet transition conditions model [47]. However, most of these models have not been verified by hardware implementations. Here we propose a physical model for the hybrid transmitting and reflecting BD-RIS that is based upon the hardware scheme shown in Fig. 4(b). Its electromagnetic performance can be characterized by using Thévenin equivalent circuits [48] and linear superposition of electromagnetic waves in free space [49].

The Thévenin equivalent model of the hybrid transmitting and reflecting BD-RIS is shown in Fig. 10. Given a BD-RIS consisting of M cells, it can be viewed as a phase reconfigurable reflecting antenna array, as enclosed by the pink dashed line box in Fig. 10, loaded with an M -port reconfigurable network, as enclosed by the blue dashed line box. The M -port reconfigurable network is further constructed by M two-port tunable power splitters cascaded with another M -element phase reconfigurable transmitting antenna array, as enclosed by the orange dashed line box.

For each phase reconfigurable antenna, there are q switches ($q = 6$ in our proposed design), so that the antenna array will have in total $q \times M = Q$ switches ($q = 6$ and $M = 16$ and therefore, $Q = 96$). To model the effect of these Q switches we can replace them by Q internal ports, as highlighted by the green dashed line. The internal ports are then terminated with equivalent loads to denote the on and off states of the switches. Thus, the entire phase reconfigurable antenna array, e.g., reflecting or transmitting antenna array, can be characterized by an $(M + Q) \times (M + Q)$ impedance matrix \mathbf{Z}_χ (where we use $\chi \in \{R, T\}$ with R and T representing the reflecting and transmitting antenna array, respectively) as

$$\mathbf{Z}_\chi = \begin{bmatrix} \mathbf{Z}_{A_\chi} & \mathbf{Z}_{A_\chi P_\chi} \\ \mathbf{Z}_{P_\chi A_\chi} & \mathbf{Z}_{P_\chi} \end{bmatrix}, \quad (18)$$

where matrix $\mathbf{Z}_{A_\chi} \in \mathbb{C}^{M \times M}$ represents the impedance sub-matrix for the M antenna ports, $\mathbf{Z}_{P_\chi} \in \mathbb{C}^{Q \times Q}$ represents the impedance sub-matrix for the Q internal ports, $\mathbf{Z}_{A_\chi P_\chi} \in \mathbb{C}^{M \times Q}$ represents the trans-impedance between the voltages of the M antenna ports and the currents of the Q internal ports, and $\mathbf{Z}_{P_\chi A_\chi}$ is the transpose of $\mathbf{Z}_{A_\chi P_\chi}$.

For the Q internal ports of the reflecting antenna, we express the load impedance at the q th internal port as $Z_{pr,q}^L$. This is based on the equivalent circuit models given in Fig. 8(b), with $Z_{pr,q}^L \in \{Z_{on}, Z_{off}\}$, where $Z_{on} = R_{on} + j\omega L$ and $Z_{off} = \frac{R_{off} + j\omega C}{R_{off} + 1/j\omega C} + j\omega L$, with $R_{on} = 1.5 \Omega$, $L = 0.7 \text{ nH}$ and $R_{off} = 2.5 \text{ k}\Omega$, $C = 0.12 \text{ pF}$. By collecting $Z_{pr,q}^L \forall q$, a diagonal matrix $\mathbf{Z}_{PR}^L = \text{diag}(Z_{pr,1}^L, \dots, Z_{pr,Q}^L)$ can be formed as marked by the black dashed line on the left side.

We also denote the load impedance of M antenna ports as $\mathbf{Z}_{AR}^L \in \mathbb{C}^{M \times M}$, which can also be viewed as the input impedance of the M -port reconfigurable network as marked by the blue dashed line in Fig. 10. Thus, we can build a block diagonal matrix $\mathbf{Z}_L = \text{blkdiag}(\mathbf{Z}_{AR}^L, \mathbf{Z}_{PR}^L) \in \mathbb{C}^{(M+Q) \times (M+Q)}$ to denote the overall load impedance matrix of this $(M + Q)$ -port network. Here $\text{blkdiag}(\cdot)$ denotes a block matrix such that the main-diagonal blocks are matrices and all off-diagonal blocks are zero matrices.

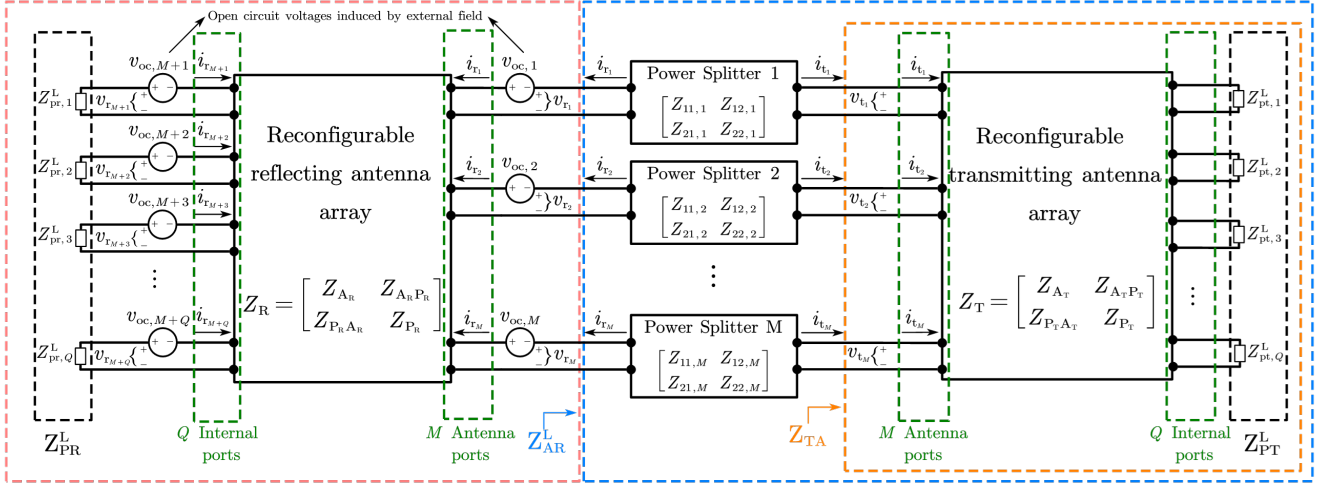


Fig. 10. Thévenin equivalent model of the hybrid transmitting and reflecting BD-RIS illuminated by an external electromagnetic field.

To analyze the entire system we denote the voltage and current vectors of the $(M + Q)$ ports embedded in the reflecting antenna array as $\mathbf{v}_R = [v_{r,1}, \dots, v_{r,M}, \dots, v_{r,M+Q}]^T$ and $\mathbf{i}_R = [i_{r,1}, \dots, i_{r,M}, \dots, i_{r,M+Q}]^T$, where T is the transpose operation. For $m = 1, \dots, M$, $v_{r,m}$ and $i_{r,m}$ refers to the voltage and current at the m th reflecting antenna, respectively, and for $q = 1, \dots, Q$, $v_{r,M+q}$ and $i_{r,M+q}$ refers to the voltage and current at the q th internal port of the reflecting antenna array, respectively. When the phase reconfigurable reflecting antenna array is illuminated by the external electromagnetic waves, \mathbf{Z}_R , \mathbf{v}_R , and \mathbf{i}_R can be related as

$$\mathbf{v}_{oc} = \mathbf{v}_R - \mathbf{Z}_R \mathbf{i}_R, \quad (19)$$

where $\mathbf{v}_{oc} = [v_{oc,1}, \dots, v_{oc,M}, \dots, v_{oc,M+Q}]^T$ with $v_{oc,m}$ and $v_{oc,M+q}$ denoting the open-circuit voltage excited at the m th antenna port and the q th internal port for $m = 1, \dots, M$, and $q = 1, \dots, Q$, respectively. For this $(M + Q)$ -port network, we also have the following relationship between \mathbf{Z}_L , \mathbf{v}_R , and \mathbf{i}_R ,

$$\mathbf{v}_R = -\mathbf{Z}_L \mathbf{i}_R. \quad (20)$$

By substituting (20) into (19), the currents at all the M antenna ports and Q internal ports of the reflecting antenna array excited by external electromagnetic waves is given by

$$\mathbf{i}_R = -(\mathbf{Z}_R + \mathbf{Z}_L)^{-1} \mathbf{v}_{oc}. \quad (21)$$

The total controllable scattered pattern, which corresponds to the total controllable reflected fields, can then be calculated using the expression

$$\mathbf{E}_r(\Omega) = \sum_{m=1}^M i_{r,m} \mathbf{E}_m(\Omega) + \sum_{q=1}^Q i_{r,M+q} \mathbf{E}_{M+q}(\Omega) + \mathbf{E}_{oc}(\Omega) - \mathbf{E}_r^{\text{str}}(\Omega), \quad (22)$$

where $\Omega = (\theta, \varphi)$ with $\theta \in [0, 180^\circ]$ and $\varphi \in [0, 360^\circ]$. $\mathbf{E}_m(\Omega)$ and $\mathbf{E}_{M+q}(\Omega)$ are the electric fields radiated by the m th reflecting antenna port and q th internal port excited by a unit current source when all the other antenna and internal ports are open-circuited, respectively. $\mathbf{E}_{oc}(\Omega)$ is the scattered

pattern when all the M antenna ports and Q internal ports are open-circuited. $\mathbf{E}_r^{\text{str}}(\Omega)$ is the structural mode scattering field when all the ports of the antenna array are conjugated-matched. Therefore, $\mathbf{E}_r(\Omega)$ also corresponds to the antenna scattering field as defined in Section IV.C.

To calculate the reflected fields, the key lies in the construction of load impedance \mathbf{Z}_L . This is because in (21) and (22), \mathbf{Z}_R , \mathbf{v}_{oc} , $\mathbf{E}_m(\Omega) \forall m$, $\mathbf{E}_{M+q}(\Omega) \forall q$, $\mathbf{E}_{oc}(\Omega)$, $\mathbf{E}_r^{\text{str}}(\Omega)$ depict the fundamental electromagnetic characteristics of the designed structure and can be acquired using electromagnetic solvers once, such as CST Microwave Studio. As part of \mathbf{Z}_L , the load impedance matrix of internal ports, \mathbf{Z}_{PR}^L can be fully constructed once the states of all the switches in the reflecting antenna array are known (see later Section), while the load impedance \mathbf{Z}_{AR}^L of M antenna ports still needs to be found.

The input impedance matrix of the loaded M -port network \mathbf{Z}_{AR}^L , consists of M two-port power splitters cascaded with the M -element reconfigurable transmitting antenna array. Denote the antenna impedance matrix of the cascaded transmitting antenna array as $\mathbf{Z}_{TA} \in \mathbb{C}^{M \times M}$, marked by the orange dashed line in Fig. 10. Define $\mathbf{v}_T = [v_{t,1}, \dots, v_{t,M}]^T$ and $\mathbf{i}_T = [i_{t,1}, \dots, i_{t,M}]^T$ to denote the voltage and current vectors of the M antenna ports embedded in the transmitting antenna array. For the transmitting antenna array, \mathbf{v}_T and \mathbf{i}_T are related by

$$\mathbf{v}_T = \mathbf{Z}_{TA} \mathbf{i}_T. \quad (23)$$

Besides, considering that each reflecting antenna and transmitting antenna are interconnected via a power splitter, for the m th power splitter, we can relate $v_{r,m}$, $i_{r,m}$ and $v_{t,m}$, $i_{t,m}$ by

$$\begin{bmatrix} v_{r,m} \\ v_{t,m} \end{bmatrix} = \begin{bmatrix} z_{11,m} & z_{12,m} \\ z_{21,m} & z_{22,m} \end{bmatrix} \begin{bmatrix} -i_{r,m} \\ -i_{t,m} \end{bmatrix}, \quad (24)$$

where each entry of the impedance matrix of power splitter $z_{ij,m}(i, j = 1, 2) \forall m$ is determined by the operation mode of the power splitters and can be obtained based on our measured S-parameters for different modes in Section IV.B. Therefore, by combining (23) and (24), the load impedance \mathbf{Z}_{AR}^L can be

interpreted as

$$\mathbf{Z}_{\text{AR}}^{\text{L}} = -(\mathbf{C} - \mathbf{Z}_{\text{TA}}\mathbf{A})^{-1}(\mathbf{Z}_{\text{TA}}\mathbf{B} - \mathbf{D}), \quad (25)$$

where $\mathbf{A} = \text{diag}(a_1, a_2, \dots, a_M)$ with $a_m = -1/z_{12,m}$, $\mathbf{B} = \text{diag}(b_1, b_2, \dots, b_M)$ with $b_m = -z_{11,m}/z_{12,m}$, $\mathbf{C} = \text{diag}(c_1, c_2, \dots, c_M)$ with $c_m = -z_{22,m}/z_{12,m}$, and $\mathbf{D} = \text{diag}(d_1, d_2, \dots, d_M)$ with $d_m = z_{22,m}z_{11,m}/z_{12,m} - z_{21,m}$, for $m = 1, \dots, M$. While \mathbf{Z}_{TA} refers to the antenna impedance matrix of the transmitting antenna array, it should be expressed by the impedance sub-matrix \mathbf{Z}_{AT} for the M transmitting antenna ports as defined from (18) and a perturbation term characterizing the effects of different phase states of transmitting antennas [50] as follows

$$\mathbf{Z}_{\text{TA}} = \mathbf{Z}_{\text{AT}} - \mathbf{Z}_{\text{ATPT}}(\mathbf{Z}_{\text{PT}} + \mathbf{Z}_{\text{PT}}^{\text{L}})^{-1}\mathbf{Z}_{\text{PTAT}}, \quad (26)$$

where \mathbf{Z}_{PT} , \mathbf{Z}_{ATPT} , \mathbf{Z}_{PTAT} are also given from (18), and similar to $\mathbf{Z}_{\text{PR}}^{\text{L}}$, we define $\mathbf{Z}_{\text{PT}}^{\text{L}} = \text{diag}(Z_{\text{pt},1}^{\text{L}}, \dots, Z_{\text{pt},Q}^{\text{L}})$ with $Z_{\text{pt},q}^{\text{L}} \in \{Z_{\text{on}}, Z_{\text{off}}\}$, $q = 1, \dots, Q$, to denote the load impedance matrix of all the Q internal ports on the transmitting antenna array, as marked by the black dashed line on the right side in Fig. 10. Hence, by calculating \mathbf{Z}_{TA} , we can include the states information of all the antenna elements on the transmitting antenna array.

Till now, $\mathbf{Z}_{\text{L}} = \text{blkdiag}(\mathbf{Z}_{\text{AR}}^{\text{L}}, \mathbf{Z}_{\text{PR}}^{\text{L}}) \in \mathbb{C}^{(M+Q) \times (M+Q)}$ can be fully expressed by collecting $\mathbf{Z}_{\text{PR}}^{\text{L}}$ and $\mathbf{Z}_{\text{AR}}^{\text{L}}$, which contains the states information of all the reflecting and transmitting antennas and the operation mode information of all the power splitters. Therefore, based on (21) and (22), for any combination of the states and any operation mode of the power splitters, the corresponding \mathbf{i}_{R} , \mathbf{v}_{R} and controllable reflected fields $\mathbf{E}_{\text{r}}(\Omega)$ can be obtained.

To calculate the transmitted fields, we can derive $i_{t,m} \forall m$ at each transmitting antenna port from (21) and (24) by

$$i_{t,m} = c_m v_{\text{r},m} + d_m i_{\text{r},m}. \quad (27)$$

Then by linear superposition of the excited electromagnetic waves at each transmitting antenna port, the overall transmitted field can be expressed as

$$\mathbf{E}_{\text{t}}(\Omega) = \sum_{m=1}^M i_{t,m} \mathbf{E}_{\text{t},m}(\Omega, \mathbf{Z}_{\text{PT}}^{\text{L}}), \quad (28)$$

where $\mathbf{E}_{\text{t},m}(\Omega, \mathbf{Z}_{\text{PT}}^{\text{L}})$ denotes the electric field radiated by the m th transmitting antenna port excited by a unit current source when all the other transmitting antenna ports are open-circuited and the Q internal ports are terminated with load impedance $\mathbf{Z}_{\text{PT}}^{\text{L}}$ according to the specific combination of phase states of transmitting antennas. Defining $\mathbf{E}_{\text{t}}(\Omega, \mathbf{Z}_{\text{PT}}^{\text{L}}) = [\mathbf{E}_{\text{t},1}(\Omega, \mathbf{Z}_{\text{PT}}^{\text{L}}), \dots, \mathbf{E}_{\text{t},M}(\Omega, \mathbf{Z}_{\text{PT}}^{\text{L}})]$, $\mathbf{E}_{\text{t}}(\Omega, \mathbf{Z}_{\text{PT}}^{\text{L}})$ can be found by [50]

$$\mathbf{E}_{\text{t}}(\Omega, \mathbf{Z}_{\text{PT}}^{\text{L}}) = \mathbf{E}_{\text{A}}(\Omega) - \mathbf{E}_{\text{P}}(\Omega)(\mathbf{Z}_{\text{PT}} + \mathbf{Z}_{\text{PT}}^{\text{L}})^{-1}\mathbf{Z}_{\text{PTAT}}, \quad (29)$$

where $\mathbf{E}_{\text{A}}(\Omega) = [\mathbf{E}_{\text{t},1}(\Omega), \dots, \mathbf{E}_{\text{t},M}(\Omega)]$ and $\mathbf{E}_{\text{P}}(\Omega) = [\mathbf{E}_{\text{t},M+1}(\Omega), \dots, \mathbf{E}_{\text{t},M+Q}(\Omega)]$ with $\mathbf{E}_{\text{t},m}(\Omega)$ and $\mathbf{E}_{\text{t},M+q}(\Omega)$ being the electric fields radiated by the m th transmitting antenna port and by the q th internal port on the transmitting antenna array excited by a unit current source when all the

other antenna and internal ports are open-circuited, respectively. \mathbf{Z}_{PT} and \mathbf{Z}_{ATPT} can be obtained from \mathbf{Z}_{T} by (18) and similarly, \mathbf{Z}_{T} , $\mathbf{E}_{\text{t},m}(\Omega) \forall m$, $\mathbf{E}_{\text{t},M+q}(\Omega) \forall q$ can also be acquired using CST Microwave Studio once.

Therefore, when a vertically incident plane wave impinges on one side of the hybrid transmitting and reflecting BD-RIS, as long as the operation mode of power splitters and the phase configurations of the reflecting and transmitting antenna arrays are settled, we can efficiently calculate the corresponding reflected and transmitted fields based on (21), (22), (27), and (28), respectively.

B. Beamforming Optimization

For the proposed BD-RIS design, for one cell with two antennas interconnected with each other through a power splitter as shown in Fig. 5, there are 16 combinations (since each antenna has four states). Therefore for a BD-RIS with 4×4 cells, a total of 16^{16} configurations are available, which is impractical for direct calculation for beam steering applications. To efficiently optimize the radiation patterns for BD-RIS operating in different modes, we adopt GA to optimize the phase states of the reflecting and transmitting antennas to achieve desired beamforming targets.

To illustrate, denote the state of the m th reflecting and transmitting antenna as $x_{\text{r},m}$ and $x_{\text{t},m}$, $m = 1, \dots, 16$, respectively. Each of them should be depicted by two binary bits to distinguish four states, i.e., $x_{\text{r},m}, x_{\text{t},m} \in \{00, 01, 10, 11\}$. Once given the specific states of $x_{\text{r},m}$ and $x_{\text{t},m}$, the corresponding load impedances, from $Z_{\text{pt},6(m-1)+1}^{\text{L}}$ to $Z_{\text{pt},6m}^{\text{L}}$, and from $Z_{\text{pt},6(m-1)+1}^{\text{L}}$ to $Z_{\text{pt},6m}^{\text{L}}$, for 6 internal ports on the m th reflecting and transmitting antenna can be found by loading different combinations of Z_{on} and Z_{off} based on the reconfigurable control states in Table I in Section IV.C, respectively. Define the phase state configuration vector as $\mathbf{x} = [x_{\text{r},1}, \dots, x_{\text{r},M}, x_{\text{t},1}, \dots, x_{\text{t},M}]^{\text{T}}$, which collects all the phase states information of the reflecting and transmitting antennas. Thus, a general optimization process can be formulated as

$$\begin{aligned} \min_{\mathbf{x}} \quad & -|E_{\text{r}}(f_{\text{c}}, \Omega_{\text{R}}, \mathbf{x})| |E_{\text{t}}(f_{\text{c}}, \Omega_{\text{T}}, \mathbf{x})| \\ \text{s.t.} \quad & \mathbf{x} \in \{00, 01, 10, 11\}^{2M}, \end{aligned} \quad (30)$$

where f_{c} is the center frequency set as 2.4 GHz for the designed BD-RIS. $\Omega_{\text{R}} = (\theta_{\text{R}}, \varphi_{\text{R}})$ and $\Omega_{\text{T}} = (\theta_{\text{T}}, \varphi_{\text{T}})$ are the two target beam angles for the reflected and transmitted radiation patterns, respectively. Taking the coordinate system shown in Fig. 1 as reference, then we have $\varphi_{\text{R}}, \varphi_{\text{T}} \in [0, 360^\circ)$, $\theta_{\text{R}} \in [0, 90^\circ)$, and $\theta_{\text{T}} \in (90^\circ, 180^\circ]$. When we design the reflection (transmission) mode, and considering that the transmitted (reflected) signals are almost negligible, we only need to conduct half-space beamforming optimization by assigning $|E_{\text{t}}|$ ($|E_{\text{r}}|$) as unity in the cost function in (30).

The optimized patterns for reflection mode and transmission mode with -45° to 45° scanning range in the YOZ plane are presented in Fig. 11(a)-(b) and (c)-(d), respectively. To verify the independent control over reflected and transmitted beams when operating in hybrid mode, the transmitted beams are fixed toward 180° or -165° when scanning the reflected beams from -30° to 30° as shown in Fig. 12(a)-(b); the

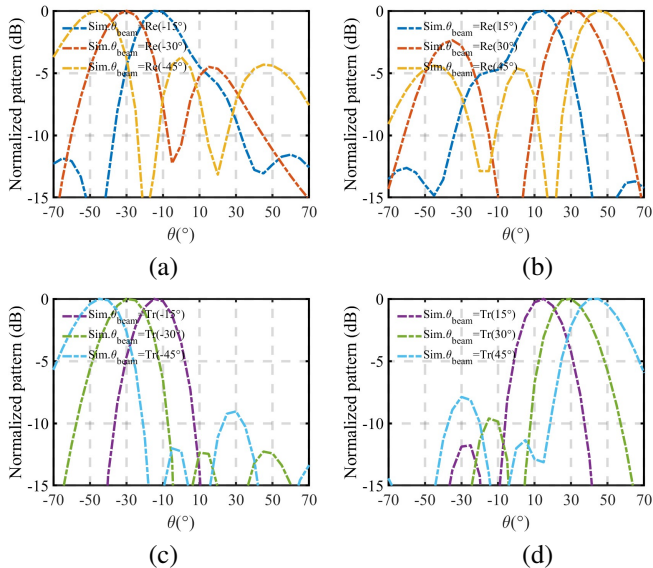


Fig. 11. Simulated normalized scattered wave pattern in the YOZ plane at 2.4 GHz with the incident wave perpendicular to the BD-RIS when the BD-RIS operates in (a) Reflection mode with scanning beams $(\theta, \phi)_{\text{Re,beam}} = (-45^\circ \sim -15^\circ, 90^\circ)$, (b) Reflection mode with scanning beams $(\theta, \phi)_{\text{Re,beam}} = (15^\circ \sim 45^\circ, 90^\circ)$, (c) Transmission mode with scanning beams $(\theta, \phi)_{\text{Tr,beam}} = (-165^\circ \sim -135^\circ, 90^\circ)$, (d) Transmission mode with scanning beams $(\theta, \phi)_{\text{Tr,beam}} = (135^\circ \sim 165^\circ, 90^\circ)$.

reflected beams are fixed toward 0° and 30° when scanning the transmitted beams from -150° to 150° as shown in Fig. 12(c)-(d). As illustrated in Section III, the effective reflection phase control of one cell is 1-bit, less than the 2-bit phase reconfigurability of transmission phase. This makes the reflected beams all feature wider beamwidth and higher sidelobes than the transmitted ones. These discrepancies can be improved by employing more powerful phase reconfigurable antennas with higher resolution and scaling up the array scale of the BD-RIS. Besides, It should be noted that, due to the symmetric characteristic of the BD-RIS with 4×4 cells, its optimized scattering performance in the XOZ plane is very similar to that of the YOZ plane. Therefore, the above results demonstrate that the 4×4 BD-RIS can realize dynamic mode switching with independent beam control.

VI. EXPERIMENTAL RESULTS

To experimentally verify the proposed BD-RIS design, we fabricated a prototype of the BD-RIS with 4×4 cells as shown in Fig. 13, where the DC control circuits are also integrated with the reflecting and transmitting antenna arrays, respectively. As illustrated in Section IV.C, we need 5 I/O pins to control one 2-bit antenna. Thus, for the BD-RIS with $4 \times 4 \times 2$ antennas, we need in total 160 pins and then three FPGAs AX7035, each of which has 64 I/O pins, are used to configure the states of all the diodes to realize the desired beamforming designs. Detailed experimental setups and results are provided as follows.

A. Experimental Setup

To measure the reflected and transmitted fields of the BD-RIS, we set up a testbed with a circular space of 6 m diameter

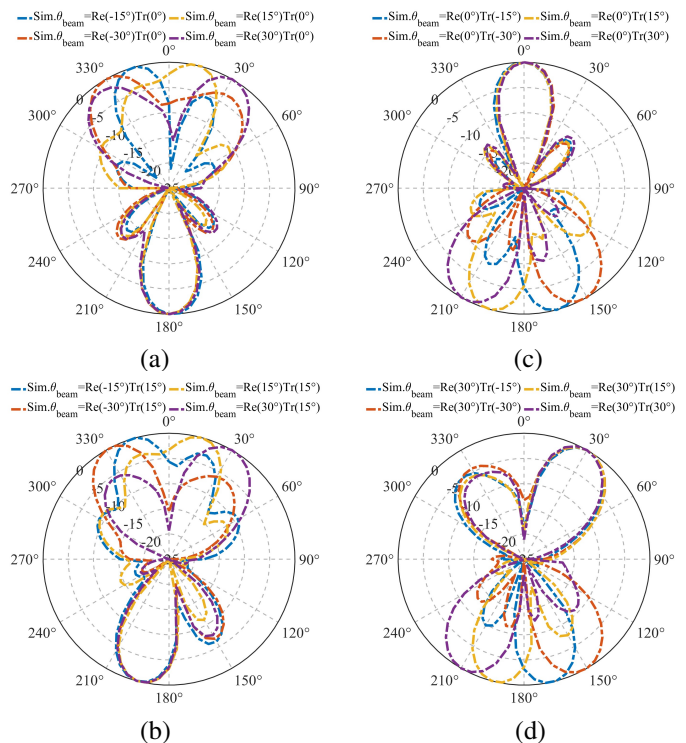


Fig. 12. Simulated normalized scattered wave pattern in the YOZ plane at 2.4 GHz with the incident wave perpendicular to the BD-RIS when the BD-RIS operates in hybrid mode. (a) Scanning reflected scattered patterns $(\theta, \phi)_{\text{Re,beam}} = (-30^\circ \sim 30^\circ, 90^\circ)$ with fixed transmitted scattered patterns $(\theta, \phi)_{\text{Tr,beam}} = (180^\circ, 90^\circ)$. (b) Scanning reflected scattered patterns $(\theta, \phi)_{\text{Re,beam}} = (-30^\circ \sim 30^\circ, 90^\circ)$ with fixed transmitted scattered patterns $(\theta, \phi)_{\text{Tr,beam}} = (-165^\circ, 90^\circ)$. (c) Scanning transmitted scattered patterns $(\theta, \phi)_{\text{Tr,beam}} = (-150^\circ \sim 150^\circ, 90^\circ)$ with fixed reflected scattered patterns $(\theta, \phi)_{\text{Re,beam}} = (0^\circ, 90^\circ)$. (d) Scanning transmitted scattered patterns $(\theta, \phi)_{\text{Tr,beam}} = (-150^\circ \sim 150^\circ, 90^\circ)$ with fixed reflected scattered patterns $(\theta, \phi)_{\text{Re,beam}} = (30^\circ, 90^\circ)$.

as shown in Fig. 14. Two horn antennas were located 3 m away from the fabricated BD-RIS, and situated within its far-field region. One horn antenna was used as the transmitter offering a vertically incident plane wave, while the other acted as a receiver to test the scattered signals by the BD-RIS. A vector network analyzer, Rohde & Schwarz ZVA40, was utilized to measure the S_{21} parameter between the transmitter and receiver. By fixing the transmitter and rotating the receiver at 5° intervals, we can measure the scattered fields of the BD-RIS over all angles.

To avoid repeatedly moving the fabricated BD-RIS and its controlling devices, while still considering the elimination of environmental effects, we propose an efficient testing method based on structural and antenna scattering as described in Section IV.C. That is we obtain

$$S_{21,\text{scat}}^{\text{ant}}(\Omega) = S_{21,\text{total}}(\Omega) - S_{21,\text{total}}^{\text{str}}(\Omega), \quad (31)$$

instead of measuring an environmental $S_{21}(\Omega)$ as in the experimental sections of [46], [51], we can keep the BD-RIS stationary and measure and subtract the corresponding structural scattering part for the reflected or transmitted waves. This is because the subtracted total structural part already

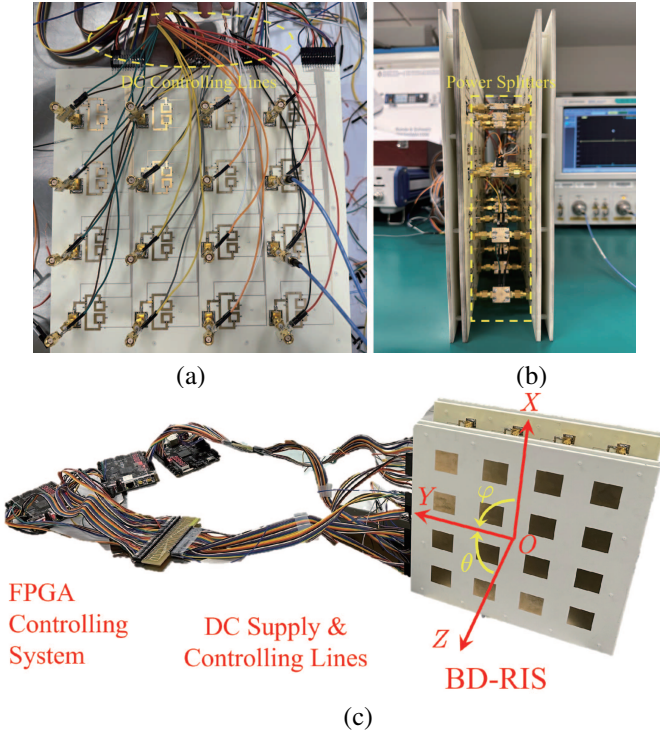


Fig. 13. Photograph of the prototype of the hybrid transmitting and reflecting BD-RIS with 4×4 cells and the controlling systems. (a) Inner view. (b) Side view. (c) Overall view.

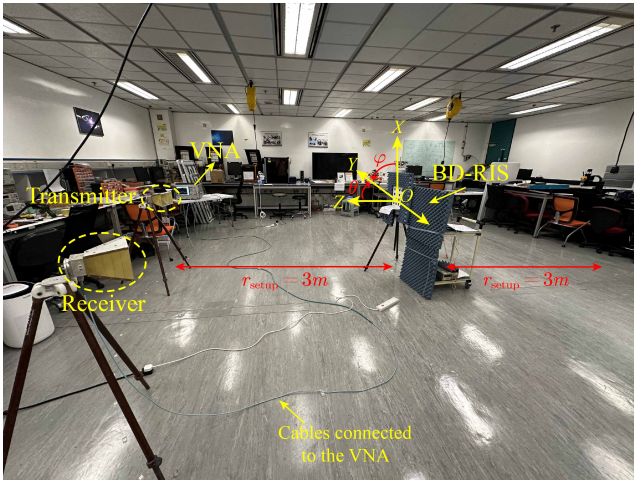


Fig. 14. Photograph of the experiment setup for measuring the reflected and transmitted radiation patterns of the hybrid transmitting and reflecting BD-RIS. The configuration of the coordinate system and its origin O are also shown.

includes the effects of the environment. In this way, the left term $S_{21, \text{scat}}^{\text{ant}} (\Omega)$ corresponds to the pure antenna scattering part. It is also consistent with our theoretical calculation by (22) and (28). As defined, the structural scattering part refers to the scattered pattern when the antenna is conjugate-matched. In the experiments, for the reflected signals, the situation where all the reflecting antennas are conjugate-matched corresponds to the situation where all the power splitters operate in transmission mode. For the transmitted waves, the situation where all the transmitting antennas are

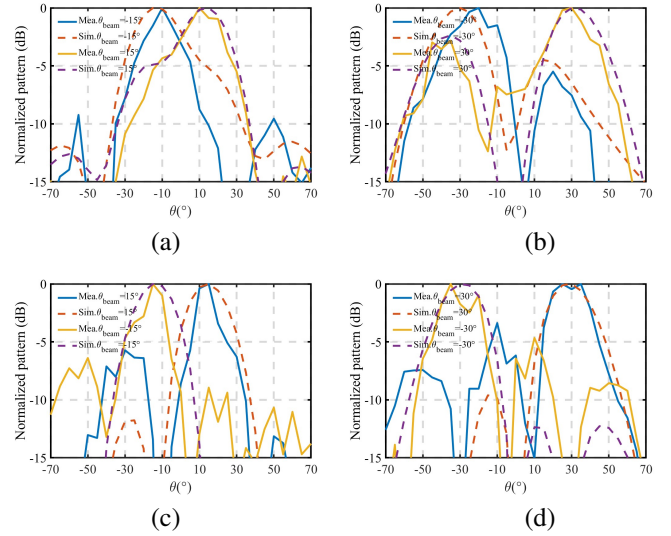


Fig. 15. Measured and simulated normalized scattered wave pattern in the YOZ plane at 2.4 GHz with the incident wave perpendicular to the BD-RIS when the BD-RIS operates in (a) Reflection mode with $(\theta, \phi)_{\text{Re,beam}} = (\pm 15^\circ, 90^\circ)$, (b) Reflection mode with $(\theta, \phi)_{\text{Re,beam}} = (\pm 30^\circ, 90^\circ)$, (c) Transmission mode with $(\theta, \phi)_{\text{Tr,beam}} = (\pm 165^\circ, 90^\circ)$, (d) Transmission mode with $(\theta, \phi)_{\text{Tr,beam}} = (\pm 150^\circ, 90^\circ)$.

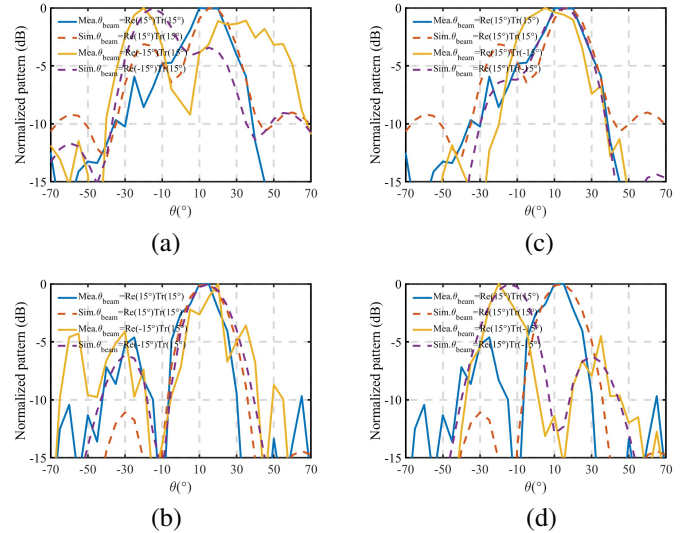


Fig. 16. Measured and simulated normalized scattered wave pattern in the YOZ plane at 2.4 GHz with the incident wave perpendicular to the BD-RIS when the BD-RIS operates in hybrid mode (a) Reflected scattered patterns when $(\theta, \phi)_{\text{Re,beam}} = (\pm 15^\circ, 90^\circ)$ and $(\theta, \phi)_{\text{Tr,beam}} = (165^\circ, 90^\circ)$, (b) Transmitted scattered patterns when $(\theta, \phi)_{\text{Re,beam}} = (\pm 15^\circ, 90^\circ)$ and $(\theta, \phi)_{\text{Tr,beam}} = (165^\circ, 90^\circ)$, (c) Reflected scattered patterns when $(\theta, \phi)_{\text{Re,beam}} = (15^\circ, 90^\circ)$ and $(\theta, \phi)_{\text{Tr,beam}} = (\pm 165^\circ, 90^\circ)$, (d) Transmitted scattered patterns when $(\theta, \phi)_{\text{Re,beam}} = (15^\circ, 90^\circ)$ and $(\theta, \phi)_{\text{Tr,beam}} = (\pm 165^\circ, 90^\circ)$.

conjugate-matched corresponds to the situation where all the power splitters operate in reflection mode.

B. Measurement Results

Fig. 15(a)-(b) show the simulated and measured scattered pattern in the YOZ plane with four representative directions

TABLE II
COMPARISON WITH RELATED WORK

Ref.	Frequency (GHz)	Reconfigurable design	Reflection mode	Hybrid mode	Transmission mode	Polarization conversion	Incident wave range	Excitation method
[21]	11.5	No	Fixed	Fixed	Fixed	Required	Single side	Near-field
[32]	4.75	No	Fixed	Fixed	Fixed	Required	Single side	Near-field
[22]	5	Yes	1-bit	/	1-bit	Not required	Single side	Near-field
[35]	9.5	Yes	1-bit	/	1-bit	Required	Single side	Near-field
[36]	5.8	Yes	/	1-bit (Re)&1-bit (Tr)	/	Required	Single side	Near-field
This work	2.4	Yes	1-bit	1-bit (Re)&2-bit (Tr)	2-bit	Not required	Dual sides	Far-field

Re: Reflection, Tr: Transmission.

of reflected beams when the BD-RIS is operating in reflection mode with a vertically incident plane wave excitation. Fig. 15(c)-(d) refers to the situation when the BD-RIS operates in transmission mode with four transmitted beams. It can be observed that the measured reflected and transmitted patterns generally agree with the simulated results utilizing (22) and (28), respectively. The small disagreement is due to the non-ideal wave excitation, background scattering, and fabrication and positioning errors. Besides, it can be observed that, the measured reflected beams also feature wider beamwidth and higher sidelobes than the transmitted ones, which align with the fact that the effective reflection phase reconfigurability is less than that of transmission phase. Anyhow, the fabricated BD-RIS can realize reflected and transmitted beam steering from -30° to 30° in the reflection and transmission space of the YOZ plane in reflection mode and transmission mode, respectively. While in this experiment our purpose is to demonstrate the viability of beam steering, wider beam steering angles will be able to be achieved using BD-RIS with more cells.

The key result for our design is the demonstration of the hybrid mode. Fig. 16 showcases the independent beam steering capabilities of the reflected and transmitted fields when the BD-RIS operates in hybrid mode. To illustrate, the left column depicts the case when the reflected beam is directed toward -15° and 15° in the reflection space shown in Fig. 15(a), while the transmitted beam is fixed toward 15° in the transmission space shown in Fig. 15(b). Conversely, the right column depicts the case when the reflected beam is fixed toward 15° as shown in Fig. 15(c), while the transmitted beam is directed toward -15° and 15° as shown in Fig. 15(d). Similarly, the beam steering performance of the transmitted pattern is still better than that of the reflected pattern in terms of thinner beamwidth and lower sidelobes. One reason for the discrepancies in the sidelobes of reflected beams in Fig. 15(a) is that the loaded impedance of the reflecting antenna array is not exactly 50Ω and therefore the structural scattering pattern of the reflected waves is not accurately modeled. Overall however these results provide solid validation for the mode switching and independent beam steering capabilities of the proposed BD-RIS.

C. Comparison with Related Work

Table II compares the performance of the proposed hybrid transmitting and reflecting BD-RIS with related work. Although all the listed previous works [21], [22], [32], [35], [36] have avoided using the frequency multiplexing technique to realize bidirectional functionalities, some of them still suffer from the limitations of being non-reconfigurable [21], [32], or involving polarization conversion [32], [35], [36]. More importantly, for the reconfigurable designs, [22], [35], [36], they can only realize the hybrid mode, or reflection or transmission mode, but cannot directly switch between the three modes and ensure independent control of the reflected and transmitted beams. In addition, none of the abovementioned works feature a symmetrical structure, which restricts their applications in real-life wireless communication environments where waves are incident from both sides. In our work, to overcome this limitation, we separate the phase and power splitting reconfigurability control by designing a 2-bit phase reconfigurable antenna and a tunable two-port power splitter. The interconnection of the identical polarization ports of the two 2-bit antennas with the two-port power splitter not only enables independent beam control and power splitting, but also keeps the polarization of reflected and transmitted waves unchanged. Furthermore, this configuration ensures a symmetrical structure. Based on our proposed architecture, the proposed BD-RIS cell can also be extended into a dual-polarized version, by using a dual-polarized phase reconfigurable antenna with two sets of two-port power splitter. This still secures independent control of each polarization, thus increasing polarization diversity.

VII. CONCLUSIONS

A reconfigurable and symmetric hybrid transmitting and reflecting BD-RIS design has been proposed, which boasts independent beam steering and mode switching capabilities among reflection, transmission and hybrid modes in the same aperture, frequency band and polarization. Based on scattering matrix analysis and guided by a novel integrated scheme, the hybrid transmitting and reflecting BD-RIS comprises two reconfigurable antenna arrays interconnected by an array of tunable two-port power splitters. The two-port power splitter is built upon a varactor parallel with a bias inductor, able to

realize mode switching with less than 1 dB insertion loss. To integrate the phase shifter with an antenna, a 2-bit phase reconfigurable antenna with 200 MHz bandwidth around 2.4 GHz, stable radiation patterns among four states and evenly distributed phases over 360° has been promoted to serve as the building block for those two reconfigurable antenna arrays facing toward the reflection and transmission spaces. To characterize and optimize the electromagnetic response of the proposed BD-RIS design, a Thévenin equivalent physical model and corresponding analytical method have been described. A prototype of the proposed BD-RIS with 4×4 cells was fabricated and measured. Simulation and experimental results have successfully verified the multifunctionalities of the hybrid transmitting and reflecting BD-RIS design. This work helps fill the gap between realizing practical hardware design and establishing accurate physical model for the hybrid transmitting and reflecting BD-RIS, enabling hybrid transmitting and reflecting BD-RIS assisted wireless communications.

REFERENCES

- [1] W. Saad, M. Bennis, and M. Chen, "A vision of 6g wireless systems: Applications, trends, technologies, and open research problems," *IEEE Network*, vol. 34, no. 3, pp. 134–142, 2019.
- [2] C.-X. Wang, X. You, X. Gao, X. Zhu, Z. Li, C. Zhang, H. Wang, Y. Huang, Y. Chen, H. Haas *et al.*, "On the road to 6g: Visions, requirements, key technologies, and testbeds," *IEEE Commun. Surv. Tutorials*, vol. 25, no. 2, pp. 905–974, 2023.
- [3] M. Di Renzo, A. Zappone, M. Debbah, M.-S. Alouini, C. Yuen, J. de Rosny, and S. Tretyakov, "Smart radio environments empowered by reconfigurable intelligent surfaces: How it works, state of research, and the road ahead," *IEEE J. Sel. Areas Commun.*, vol. 38, no. 11, pp. 2450–2525, 2020.
- [4] Q. Wu and R. Zhang, "Towards smart and reconfigurable environment: Intelligent reflecting surface aided wireless network!" *IEEE Commun. Mag.*, vol. 58, no. 1, pp. 106–112, 2019.
- [5] Q. Wu, S. Zhang, B. Zheng, C. You, and R. Zhang, "Intelligent reflecting surface-aided wireless communications: A tutorial," *IEEE Trans. Commun.*, vol. 69, no. 5, pp. 3313–3351, 2021.
- [6] H. Li, S. Shen, and B. Clerckx, "Beyond diagonal reconfigurable intelligent surfaces: From transmitting and reflecting modes to single-, group-, and fully-connected architectures," *IEEE Trans. Wireless Commun.*, vol. 22, no. 4, pp. 2311–2324, 2022.
- [7] H. Li, S. Shen, M. Nerini, and B. Clerckx, "Reconfigurable intelligent surfaces 2.0: Beyond diagonal phase shift matrices," *IEEE Commun. Mag.*, 2023.
- [8] Y. Zhou, Y. Liu, H. Li, Q. Wu, S. Shen, and B. Clerckx, "Optimizing power consumption, energy efficiency, and sum-rate using beyond diagonal ris a unified approach," *IEEE Trans. Wireless Commun.*, vol. 23, no. 7, pp. 7423–7438, 2023.
- [9] H. Li, S. Shen, M. Nerini, M. Di Renzo, and B. Clerckx, "Beyond diagonal reconfigurable intelligent surfaces with mutual coupling: Modeling and optimization," *IEEE Commun. Lett.*, vol. 28, no. 4, pp. 937–941, 2024.
- [10] J. Xu, Y. Liu, X. Mu, and O. A. Dobre, "Star-ris: Simultaneous transmitting and reflecting reconfigurable intelligent surfaces," *IEEE Commun. Lett.*, vol. 25, no. 9, pp. 3134–3138, 2021.
- [11] S. Zhang, H. Zhang, B. Di, Y. Tan, Z. Han, and L. Song, "Beyond intelligent reflecting surfaces: Reflective-transmissive metasurface aided communications for full-dimensional coverage extension," *IEEE Trans. Veh. Technol.*, vol. 69, no. 11, pp. 13 905–13 909, 2020.
- [12] X. Mu, Y. Liu, L. Guo, J. Lin, and R. Schober, "Simultaneously transmitting and reflecting (star) ris aided wireless communications," *IEEE Trans. Wireless Commun.*, vol. 21, no. 5, pp. 3083–3098, 2021.
- [13] H. Zhang and B. Di, "Intelligent omni-surfaces: Simultaneous refraction and reflection for full-dimensional wireless communications," *IEEE Commun. Surv. Tutorials*, vol. 24, no. 4, pp. 1997–2028, 2022.
- [14] M. Ahmed, A. Wahid, S. S. Laique, W. U. Khan, A. Ihsan, F. Xu, S. Chatzinotas, and Z. Han, "A survey on star-ris: Use cases, recent advances, and future research challenges," *IEEE Internet Things J.*, vol. 10, no. 16, pp. 14 689–14 711, 2023.
- [15] H. Niu, Z. Chu, F. Zhou, P. Xiao, and N. Al-Dhahir, "Weighted sum rate optimization for star-ris-assisted mimo system," *IEEE Trans. Veh. Technol.*, vol. 71, no. 2, pp. 2122–2127, 2021.
- [16] M. Katwe, K. Singh, B. Clerckx, and C.-P. Li, "Improved spectral efficiency in star-ris aided uplink communication using rate splitting multiple access," *IEEE Trans. Wireless Commun.*, vol. 22, no. 8, pp. 5365–5382, 2023.
- [17] H. L. Wang, H. F. Ma, M. Chen, S. Sun, and T. J. Cui, "A reconfigurable multifunctional metasurface for full-space control of electromagnetic waves," *Adv. Funct. Mater.*, vol. 31, no. 25, p. 2100275, 2021.
- [18] L. Bao, Q. Ma, R. Y. Wu, X. Fu, J. Wu, and T. J. Cui, "Programmable reflection–transmission shared-aperture metasurface for real-time control of electromagnetic waves in full space," *Adv. Sci.*, vol. 8, no. 15, p. 2100149, 2021.
- [19] Q. Hu, J. Zhao, K. Chen, K. Qu, W. Yang, J. Zhao, T. Jiang, and Y. Feng, "An intelligent programmable omni-metasurface," *Laser Photonics Rev.*, vol. 16, no. 6, p. 2100718, 2022.
- [20] T. Yin, J. Ren, B. Zhang, P. Li, Y. Luan, and Y. Yin, "Reconfigurable transmission-reflection-integrated coding metasurface for full-space electromagnetic wavefront manipulation," *Adv. Opt. Mater.*, vol. 12, no. 2, p. 2301326, 2024.
- [21] K. Duan, K. Chen, T. Jiang, J. Zhao, and Y. Feng, "Non-interleaved bidirectional metasurface for spatial energy allocation," *IEEE Trans. Antennas Propag.*, 2024.
- [22] T. Yin, J. Ren, Y. Chen, K. Xu, and Y. Yin, "Highly integrated reconfigurable shared-aperture em surface with multifunctionality in transmission, reflection and absorption," *IEEE Trans. Antennas Propag.*, 2024.
- [23] L. Bao, X. Fu, R. Y. Wu, Q. Ma, and T. J. Cui, "Full-space manipulations of electromagnetic wavefronts at two frequencies by encoding both amplitude and phase of metasurface," *Adv. Mater. Technol.*, vol. 6, no. 4, p. 2001032, 2021.
- [24] X. Wang, J. Ding, B. Zheng, S. An, G. Zhai, and H. Zhang, "Simultaneous realization of anomalous reflection and transmission at two frequencies using bi-functional metasurfaces," *Sci. Rep.*, vol. 8, no. 1, p. 1876, 2018.
- [25] H.-X. Xu, S. Tang, G.-M. Wang, T. Cai, W. Huang, Q. He, S. Sun, and L. Zhou, "Multifunctional microstrip array combining a linear polarizer and focusing metasurface," *IEEE Trans. Antennas Propag.*, vol. 64, no. 8, pp. 3676–3682, 2016.
- [26] T. Cai, G. Wang, S. Tang, H. Xu, J. Duan, H. Guo, F. Guan, S. Sun, Q. He, and L. Zhou, "High-efficiency and full-space manipulation of electromagnetic wave fronts with metasurfaces," *Phys. Rev. Appl.*, vol. 8, no. 3, p. 034033, 2017.
- [27] H. Hou, G. Wang, H. Li, W. Guo, and T. Cai, "Helicity-dependent metasurfaces employing receiver-transmitter meta-atoms for full-space wavefront manipulation," *Opt. Express*, vol. 28, no. 19, pp. 27 575–27 587, 2020.
- [28] L.-X. Wu, K. Chen, T. Jiang, J. Zhao, and Y. Feng, "Circular-polarization-selective metasurface and its applications to transmit-reflect-array antenna and bidirectional antenna," *IEEE Trans. Antennas Propag.*, vol. 70, no. 11, pp. 10 207–10 217, 2022.
- [29] L. Zhang, R. Y. Wu, G. D. Bai, H. T. Wu, Q. Ma, X. Q. Chen, and T. J. Cui, "Transmission-reflection-integrated multifunctional coding metasurface for full-space controls of electromagnetic waves," *Adv. Funct. Mater.*, vol. 28, no. 33, p. 1802205, 2018.
- [30] C. Zhang, J. Gao, X. Cao, S.-J. Li, H. Yang, and T. Li, "Multifunction tunable metasurface for entire-space electromagnetic wave manipulation," *IEEE Trans. Antennas Propag.*, vol. 68, no. 4, pp. 3301–3306, 2019.
- [31] W.-L. Guo, K. Chen, G.-M. Wang, X.-Y. Luo, Y.-J. Feng, and C.-W. Qiu, "Transmission–reflection-selective metasurface and its application to rcs reduction of high-gain reflector antenna," *IEEE Trans. Antennas Propag.*, vol. 68, no. 3, pp. 1426–1435, 2019.
- [32] G. Li, H. Shi, J. Yi, B. Li, A. Zhang, and Z. Xu, "Transmission–reflection-integrated metasurfaces design for simultaneous manipulation of phase and amplitude," *IEEE Trans. Antennas Propag.*, vol. 70, no. 7, pp. 6072–6077, 2022.
- [33] J. Y. Lau and S. V. Hum, "A planar reconfigurable aperture with lens and reflectarray modes of operation," *IEEE Trans. Microwave Theory Tech.*, vol. 58, no. 12, pp. 3547–3555, 2010.
- [34] M. Wang, S. Xu, F. Yang, and M. Li, "A 1-bit bidirectional reconfigurable transmit-reflect-array using a single-layer slot element with pin

- diodes," *IEEE Trans. Antennas Propag.*, vol. 67, no. 9, pp. 6205–6210, 2019.
- [35] H. Yu, P. Li, J. Su, Z. Li, S. Xu, and F. Yang, "Reconfigurable bidirectional beam-steering aperture with transmitarray, reflectarray, and transmit-reflect-array modes switching," *IEEE Trans. Antennas Propag.*, vol. 71, no. 1, pp. 581–595, 2022.
- [36] M. Xiang, Y. Xiao, J. Deng, S. Xu, and F. Yang, "Simultaneous transmitting and reflecting reconfigurable array (star-ra) with independent beams," *IEEE Trans. Antennas Propag.*, 2023.
- [37] Y. Zhao, D. Wang, H. Gu, P. Chen, Y. Liang, M. Du, W. Liu, and L. Ge, "Design of a novel wideband reconfigurable transmit-reflect-array antenna utilizing twin lines," *IEEE Trans. Antennas Propag.*, 2024.
- [38] X. Cao, C. Deng, Y. Yin, Y. Hao, and K. Sarabandi, "1-bit reconfigurable transmit-and reflect-array antenna using patch-ground-patch structure," *IEEE Antennas Wirel. Propag. Lett.*, vol. 23, no. 1, pp. 434–438, 2023.
- [39] X. Li, Q. Huang, L. Yang, M. Cai, S. Yang, S. Yang, and Y. Li, "Dual-band wideband reflect-transmit-array with different polarizations using three-layer elements," *IEEE Antennas Wirel. Propag. Lett.*, vol. 20, no. 7, pp. 1317–1321, 2021.
- [40] S. Yang, Z. Yan, T. Zhang, M. Cai, F. Fan, and X. Li, "Multifunctional tri-band dual-polarized antenna combining transmitarray and reflectarray," *IEEE Trans. Antennas Propag.*, vol. 69, no. 9, pp. 6016–6021, 2021.
- [41] S. Liu and Q. Chen, "A wideband, multifunctional reflect-transmit-array antenna with polarization-dependent operation," *IEEE Trans. Antennas Propag.*, vol. 69, no. 3, pp. 1383–1392, 2020.
- [42] J. Feng, Z. Yan, S. Yang, F. Fan, T. Zhang, X. Liu, X. Zhao, and Q. Chen, "Reflect–transmit-array antenna with independent dual circularly polarized beam control," *IEEE Antennas Wirel. Propag. Lett.*, vol. 22, no. 1, pp. 89–93, 2022.
- [43] W. Li, Y. Wang, S. Sun, and X. Shi, "An fss-backed reflection/transmission reconfigurable array antenna," *IEEE Access*, vol. 8, pp. 23 904–23 911, 2020.
- [44] X. Zhong, H.-X. Xu, L. Chen, W. Li, H. Wang, and X. Shi, "An fss-backed broadband phase-shifting surface array with multimode operation," *IEEE Trans. Antennas Propag.*, vol. 67, no. 9, pp. 5974–5981, 2019.
- [45] C. A. Balanis, *Antenna theory: analysis and design*. John Wiley & Sons, 2016.
- [46] J. Rao, Y. Zhang, S. Tang, Z. Li, C.-Y. Chiu, and R. Murch, "An active reconfigurable intelligent surface utilizing phase-reconfigurable reflection amplifiers," *IEEE Trans. Microwave Theory Tech.*, vol. 71, no. 7, pp. 3189–3202, 2023.
- [47] J. Xu, Y. Liu, X. Mu, J. T. Zhou, L. Song, H. V. Poor, and L. Hanzo, "Simultaneously transmitting and reflecting intelligent omni-surfaces: Modeling and implementation," *IEEE Veh. Technol. Mag.*, vol. 17, no. 2, pp. 46–54, 2022.
- [48] J. Mautz and R. Harrington, "Modal analysis of loaded n-port scatterers," *IEEE Trans. Antennas Propag.*, vol. 21, no. 2, pp. 188–199, 1973.
- [49] C. A. Balanis, *Advanced engineering electromagnetics*. John Wiley & Sons, 2012.
- [50] Y. Zhang, S. Shen, Z. Han, C.-Y. Chiu, and R. Murch, "Compact mimo systems utilizing a pixelated surface: Capacity maximization," *IEEE Trans. Veh. Technol.*, vol. 70, no. 9, pp. 8453–8467, 2021.
- [51] J. Rao, Y. Zhang, S. Tang, Z. Li, S. Shen, C.-Y. Chiu, and R. Murch, "A novel reconfigurable intelligent surface for wide-angle passive beam-forming," *IEEE Trans. Microwave Theory Tech.*, vol. 70, no. 12, pp. 5427–5439, 2022.